Materials and Design 202 (2021) 109583

Contents lists available at ScienceDirect

Materials and Design

journal homepage: www.elsevier.com/locate/matdes

Evaluation and correction of cutting position's effects on quality indicator measurement of self-piercing riveted joint

Yunpeng Liu [a], Li Han [b], Huan Zhao [a], Xianping Liu [a,*]

[a] School of Engineering, University of Warwick, Coventry CV4 7AL, UK
[b] Hansher Consulting Ltd., Coventry, UK

HIGHLIGHTS

- The offset distance leads to an overestimated interlock while the rotation angle causes an underestimated interlock.
- The relative interlock error is −5%–5% with the offset distance smaller than 1.0 mm and the rotation angle less than 10°.
- The proposed correction strategy effectively reduced the relative interlock error to 1%–3%.
- Larger errors of remaining bottom sheet thickness were found around the joint central area than around the rivet tip.

GRAPHICAL ABSTRACT

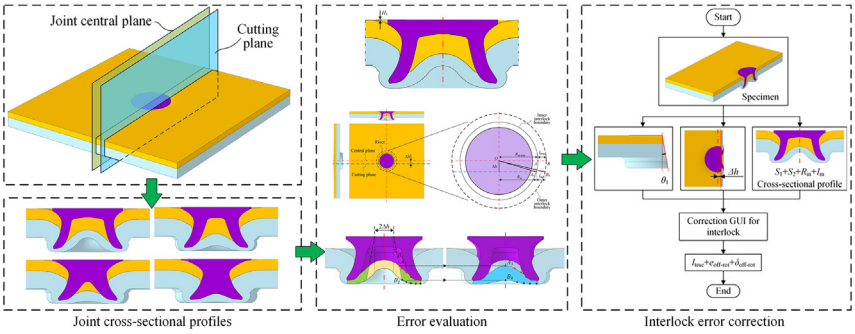

ARTICLE INFO

Article history:
Received 14 January 2021
Received in revised form 2 February 2021
Accepted 10 February 2021
Available online 14 February 2021

Keywords:
Cutting position
Error compensation
Measurement error
Quality evaluation
SPR joint

ABSTRACT

This study systematically investigated the influences of cutting positions on the measurement accuracy of the self-piercing riveted joint quality indicators. Evaluation and correction methods were proposed for the first time to estimate and compensate the interlock error caused by improper cutting positions. It was found that the measurement accuracy of the rivet head height was not influenced, but the accuracy of the interlock and the remaining bottom sheet thickness were affected by the joint cutting position. A pure offset distance could lead to an overestimated interlock while a solo rotation angle could result in an underestimated interlock. For the studied joint configurations, the relative interlock error was found in the range of −5%–5% with the offset distance smaller than 1.0 mm and the rotation angle less than 10°. The offset distance and rotation angle can cause larger errors on the remaining bottom sheet thickness around the joint central area than around the rivet tip. Moreover, the proposed correction strategy for the interlock has been proved effective and the relative interlock error could be reduced to 1%–3%.

© 2021 Published by Elsevier Ltd. This is an open access article under the CC BY-NC-ND license (http://creativecommons.org/licenses/by-nc-nd/4.0/).

1. Introduction

After many years' development, the self-piercing riveting (SPR) has become a very reliable joining technique for thin-walled structures [1]. Fig. 1 illustrates the four steps of the SPR process: firstly, the top and bottom sheets are clamped together by the blank-holder and the die to limit their relative movement during the joining process. Then, the punch moves downward and presses the rivet into the sheets. The rivet shank first pierces through the top sheet and then flares into the bottom sheet. Finally, the punch and the blank-holder move backward

* Corresponding author.
E-mail address: X.Liu@warwick.ac.uk (X. Liu).

https://doi.org/10.1016/j.matdes.2021.109583
0264-1275/© 2021 Published by Elsevier Ltd. This is an open access article under the CC BY-NC-ND license (http://creativecommons.org/licenses/by-nc-nd/4.0/).

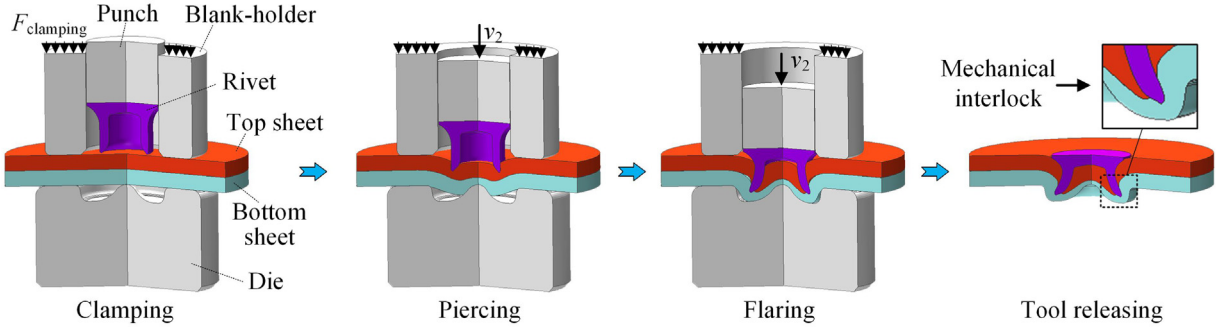

Fig. 1. Schematic of the four steps during the self-pierce riveting process.

and one SPR joint with a mechanical interlock between the bottom sheet and the rivet shank is formed. The SPR is capable of connecting similar and dissimilar materials [2], such as aluminium alloys, steels and even composite materials. It is not only suitable for two-layer stacks but also can be extended to connect three or more layer substrates [3]. This joining process usually takes 1– 4 s, and can be easily monitored by comparing the force-displacement curve of each joint with the referenced one in practical applications [4]. The SPR joining system is very convenient to be integrated into the automation production line. Due to these advantages, the SPR technique has been widely employed in many industrial sectors, especially in automotive industry.

During the SPR process, joining parameters that affect the deformation behaviours of the rivet and sheets would inevitably influence the final joint quality [5]. The sheet parameters, such as the material, thickness, number of layers and sequences, are very critical for the SPR joint quality, and thus received a lot of attentions. Fratini et al. [6] studied the possibility to join aluminium alloy AA6082-T6 and fiberglass composite sheets using the SPR technique. Abe et al. [7] explored the rivetability of high tensile strength steel and aluminium alloy AA5052-H34 sheets with the conventional rivet and die. Ma et al. [8] experimentally studied the influences of top sheet thickness on the SPR process. The results revealed that a thicker top sheet could entrap more rivet shank and significantly prevent the rivet shank flare along radial direction. Kam et al. [9] studied the effects of sheet sequence on the quality of SPR joints with vibration-damping steel and Al5052-H32 sheets. It was found that a better joint quality was achieved when the vibration-damping steel was used as the bottom sheet. In addition, the rivet parameters, such as the material, rivet length, diameter, and rivet shank profile, are also major factors affecting the joint quality, and attracted many researchers' interest. Hoang et al. [10] investigated the possibility of joining aluminium alloy 6060 sheets with different aluminium alloy rivets (i.e. 6082-T6, 7108-T5 and 7287-T6). Ma et al. [8] examined the effects of rivet length on the joint quality. Van Hall et al. [11] found that the intentional surface decarburization of the rivet can prevent the formation of fractures along the rivet leg periphery, while maintaining sufficient column strength to pierce through the sheet without buckling of the rivet shank. Li et al. [12] explored the influences of the rivet shank geometry on the joint quality. Moreover, die parameters, such as the diameter, depth and pip height, also impose significant impacts on the joint quality [13]. This has already become a research highlight of the SPR technique in the industrial and academic fields. Kam et al. [9] studied the effects of the die type on the quality of SPR joints with vibration-damping steel and Al5052-H32 sheets. It was found that the flat die showed a better performance than the pip die. The interlock showed a decreasing trend with the increment of die taper angle and die diameter. Pickin et al. [14] experimentally investigated the influences of die depth and diameter on the rivet shank flaring ratio in SPR joints. The influences of other riveting parameters, such as the joining speed, clamping force and surface conditions, on the joint quality were also reported by scholars. Using an electromagnetic self-piercing riveting (*E*-SPR) system and a universal testing machine, Liang et al. [15] studied the influences of the joining speed on the joint quality. Li [16] investigated the effects of the friction coefficient between the top and bottom sheets on the SPR process by modifying the surfaces of the top sheet with different impression tools and garnet particles. Karim et al. [17] explored the effects of the rivet coatings on the joint quality, and the results revealed that the friction properties of the rivet coatings remarkably affected the joint quality. Till now, the experimental SPR test is still the dominating approach for the research of SPR technique, and has been widely adopted in the design and quality optimization of new SPR joints. Comprehensive reviews about the research progresses of the SPR technique can be found in [18] [19].

The SPR joint quality is usually evaluated by three quality indicators measured on the joint cross-sectional profile as shown in Fig. 2: the rivet head height (H_1), the interlock (I), and the minimum remaining bottom sheet thickness (T_{min}). The H_1 directly influences the cosmetic appearance and corrosion resistance of the connected structure. According to the study of [20], the H_1 also determines the final position of the rivet inserted into the substrates and therefore affects the final magnitudes of the interlock and T_{min}. The I is very critical for the mechanical strengths [8] and failure behaviours of SPR joints. Too small interlock might lead to pull-out failures of the rivet shank from the bottom sheet [9]. The T_{min} is also critical for the corrosion performance and strengths of the SPR joint. Zhang et al. [21] reported that fatigue failure may occurred on the bottom sheet if the T_{min} was too small. The assessment criteria for the three indicators varies based on the application requirements in different industry sectors. For example, according to the standard of a world-leading car manufacturer [18], the H_1 should be between 0.3 mm and − 0.5 mm. The interlock should be greater than 0.4 mm for joints with aluminium alloy bottom sheet and greater than 0.2 mm with a steel bottom sheet. The T_{min} should be always greater than 0.2 mm and fracture of the bottom sheet should be avoided [20].

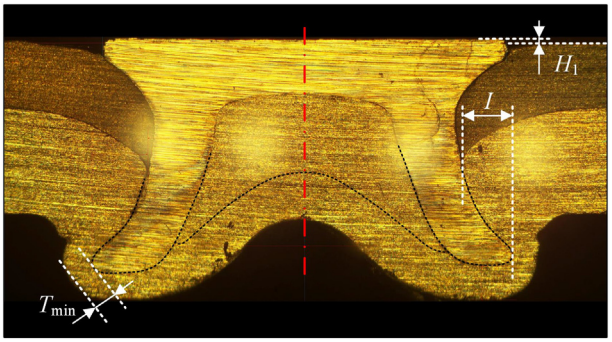

Fig. 2. Three joint quality indicators measured on the cross-sectional profile of SPR joints.

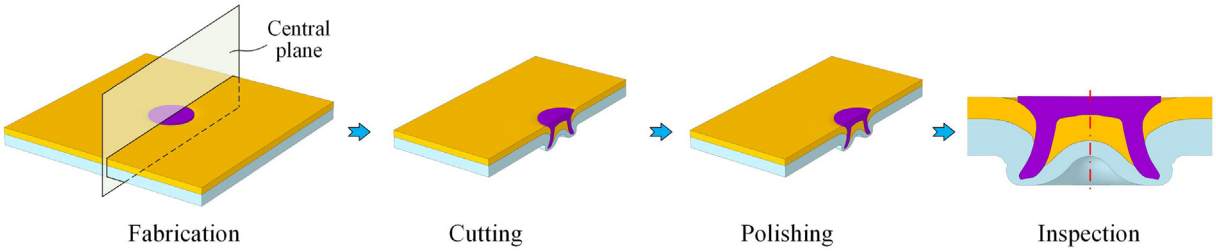

Fig. 3. Quality evaluation procedures for SPR joints.

Therefore, the accuracy of the captured joint cross-sectional profile is very important for the joint quality evaluation. Fig. 3 illustrates the procedures to experimentally get the cross-sectional profile of SPR joints, including the specimen manufacture, specimen cutting, sectioned surface polishing and cross-sectional profile inspection. Under the ideal condition, the specimen is cut along the joint central plane, and true values of the three quality indicators are measured on the captured cross-sectional profile. However, during the experimental tests, many factors would affect the cutting position, such as the specimen shape, the specimen clamping position and the wear of grinding wheel. Thus, it is very difficult to experimentally cut the specimen through the joint central plane. The misalignment between the cutting plane and the joint central plane would inevitably affect the accuracy of the captured joint cross-sectional profile, and bring measurement errors to the three quality indicators. By standardizing the specimen size and using specially designed fixtures during the riveting and cutting processes, this misalignment could be effectively reduced and the influences on the joint quality indicators could also be minimized. However, these special fixtures may become not workable under some situations. For example, the SPR joints cut from the vehicle body-in-white (BIW) (as shown in Fig. 4) usually have a nonstandard size/shape, and thus can only be sectioned roughly based on the operator's experience. Moreover, improper polishing operation for the sectioned surface may further aggravate such misalignment. Consequently, the specimen preparation, especially the improper cutting operation, will cause errors to the captured joint cross-sectional profile and the three quality indicators.

Recent years, finite element (FE) models of SPR process have been successfully developed to predict the joint quality. For example, Huang et al. [22] established a two-dimensional (2D) model of SPR joints with aluminium alloy 6111-T4 top sheet and steel HSLA340 bottom sheet. Both of the strain rate and temperature effects were considered. A reasonable agreement between the numerical and experimental results was found by comparing the joint cross-sectional profiles. Hirsch et al. [23] successfully developed a three-dimensional (3D) model to predict the quality of SPR joints with fibre reinforced polymer and metals sheets. Different from experimental SPR tests, the cutting operation carried out in the FE software would not affect the measurement accuracy of the three quality indicators, because the simulated specimens can be exactly cut along the joint central plane. However, experimental SPR tests are still required for the calibration and validation of FE models [24]. The errors from the specimen preparation stage during experimental SPR tests would therefore indirectly affect the prediction accuracy of the developed SPR simulation model. Therefore, a better understanding of the specimen preparation's (especially the specimen cutting) influences on the joint cross-sectional profile and the quality indicators will be also benefit for the development of FE models.

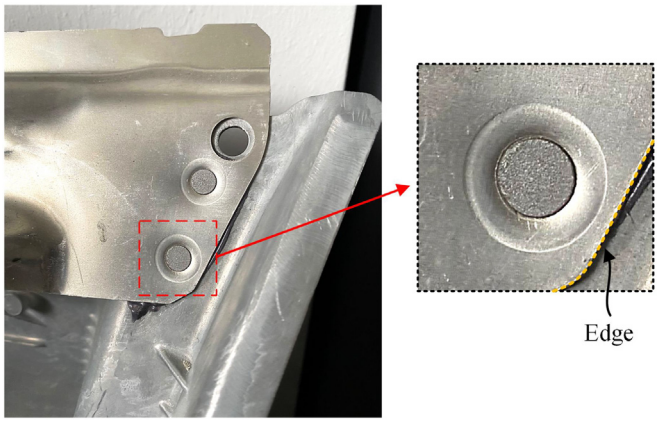

Fig. 4. SPR joints on the car body-in-white (BIW) structure.

However, although the specimen preparation is so important for the SPR joint quality evaluation and for the FE model development, to the authors' knowledge, there is still no report devoted to this issue in the public domain. The reliability of the joint quality evaluation result would be doubtful without considering the impact of improper specimen cutting position on the measurement accuracy of joint quality indicators. It will be a big contribution for the practical applications of SPR technique if effective approaches could be proposed to evaluate and compensate the measurement errors of joint quality indicators caused by the improper specimen cutting position. Therefore, in this study, the improper cutting position induced distortions of joint cross-sectional profiles were qualitatively compared and discussed. Then, the influences of improper cutting positions on the measurement accuracy of the rivet head height (H_1), interlock (I) and remaining bottom sheet thickness were systematically investigated. A mathematic model was developed to estimate the interlock errors under different cutting conditions. The impacts of the cutting position on the remaining bottom sheet thickness were also analysed and discussed in detail. To compensate the interlock error caused by the improper cutting positions, a correction/compensation approach was proposed by measuring the offset distance (Δh) and the rotation angle (θ_1) between the cutting plane and the joint central plane. Two graphical user interfaces (GUI) for the interlock error estimation and correction were also developed to facilitate practical applications. Finally, experimental SPR tests were carried out to estimate the interlock error levels for physical SPR joints and verify the performance of the proposed interlock error correction method. The conclusions drawn from this study not only give a clear understanding of the specimen cutting position's impacts on the three joint quality indicators, but also provide some useful guidelines for specimen cutting in practical applications.

2. Improper specimen cutting

During the specimen preparation process, the improper polishing operation for the sectioned surface may also affect the captured joint cross-sectional profile and the joint quality. For clarity, in this study, the error induced by the improper specimen polishing is also regarded as the error caused by the specimen cutting.

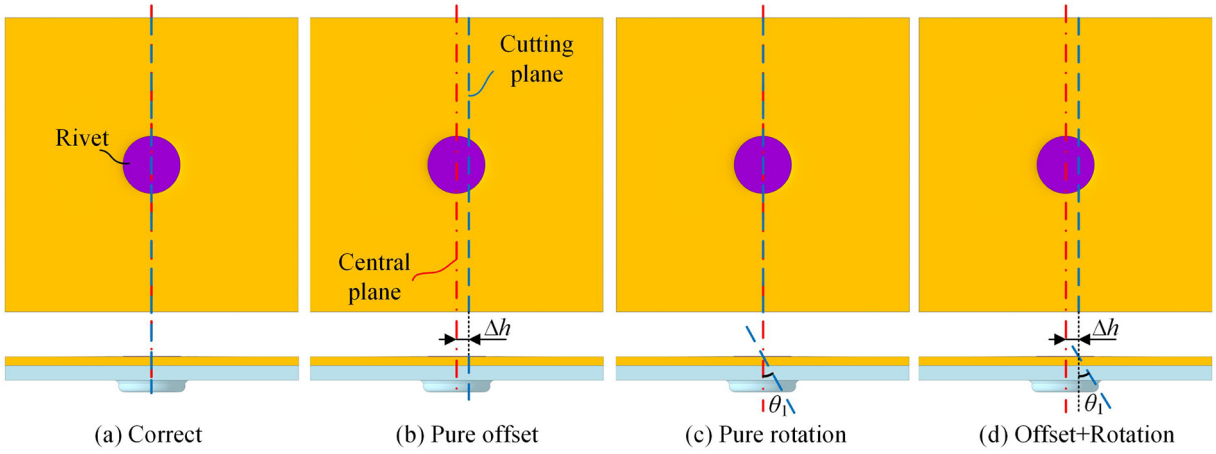

Fig. 5. The ideal specimen cutting position and three improper cutting positions: (a) Correct position, (b) Pure offset, (c) Pure rotation and (d) Offset+Rotation.

2.1. Types of improper cutting position

Under ideal conditions, as shown in Fig. 5(a), the SPR joint is exactly cut along the joint central plane (Red line). The joint central plane and the cutting plane (Blue line) coincide with each other. However, a misalignment always exists between these two planes in any experimental SPR test. Gerstmann and Awiszus [25] reported the slight misalignment between the two planes when measuring the quality indicators of flat-clinch joints. According to the relative positions, the improper specimen cutting positions can be divided into three types: (1) Pure offset in Fig. 5(b), the two planes are parallel but with a offset distance (Δh); (2) Pure rotation in Fig. 5(c), the cutting plane passes through the central line of the rivet head but had a rotation angle (θ_1) against the joint central plane; (3) Offset+Rotation in Fig. 5(d), there is an offset distance (Δh) as well as a rotation angle (θ_1) between the two planes.

2.2. Influences on the joint cross-sectional profile

Taking the SPR joint with the 1.2 mm + 2.0 mm AA5754 sheets and the 6.0 mm long boron steel rivet as an example, the joint cross-sectional profiles at different cutting positions were captured using software SolidWorks 2018. As shown in Fig. 6, a 3D joint model was first created based on the experimentally observed joint cross-sectional profile. Then, this 3D model was virtually sectioned at different cutting positions, and all the corresponding joint cross-sectional profiles were recorded. The accuracy of the tested joint profile would not affect the reliability of the conclusions made in this section. Because all the analyses were carried out based on the 3D joint model rather than the experimentally tested joint. The joint appearances and cross-sectional profiles with the pure offset distances (Δh) and pure rotation angles (θ_1) are given in Figs. 7 and 8 respectively.

As shown in Fig. 7, when the Δh is smaller than 1.0 mm, it is not easy to identify the occurrence of cutting offset by visually observing the joint appearance and the cross-sectional profile. The rivet profile (Purple region) kept almost the same when the Δh increased from 0.0 mm to 1.0 mm. In contrast, when the Δh becomes greater than 1.0 mm, the rivet profile changed a lot compared to that without the cutting offset ($\Delta h = 0$ mm). The severe distortion of rivet profile and the captured outside surface of bottom sheet (Zone 1) clearly indicated the occurrence of cutting offset. For the joint quality, the Δh showed no influence on the rivet head height (H_1) because the relative positions between the upper surfaces of the rivet and top sheet were not affected, but imposed significant influences on the remaining bottom sheet thickness. The Δh also showed some impacts on the interlock and this will be discussed later.

Compared with the cutting offset distance, the occurrence of cutting rotation angle is easier to be visually identified from the joint appearance but still difficult to be discovered from the joint cross-sectional profile as shown in Fig. 8. When the θ_1 is less than 10°, the joint cross-sectional profile kept almost the same. When the θ_1 becomes larger than 10°, obvious changes of the remaining bottom sheet thickness were noticed. The changes of rivet profile become evident when the θ_1 increases to 20° and 25°. It was also discovered that the θ_1 imposed a larger influence on the bottom half than on the upper half of the joint cross-sectional profile. This is because the cutting plane passes through the central line of the rivet head, and the points on the cutting plane have different distances to the joint central plane. A larger distance resulted in a greater distortion between the joint profiles captured on the joint central plane and on the cutting plane. For the joint quality, the θ_1 also showed no influence on the rivet head height (H_1) but imposed obvious influences on the interlock and on the remaining bottom sheet thickness.

When the cutting offset and cutting rotation happen at the same time, a superimposed effect would be imposed on the joint cross-

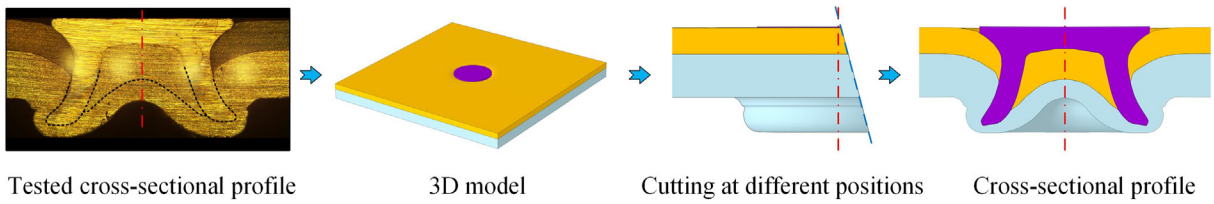

Fig. 6. Procedures to get the joint cross-sectional profiles virtually at different cutting positions.

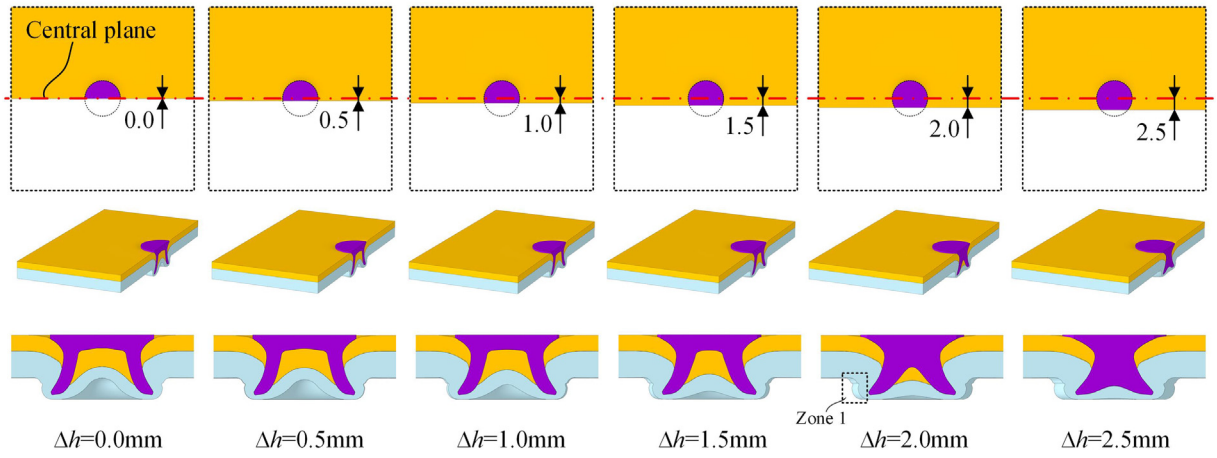

Fig. 7. Joint appearances and cross-sectional profiles at different pure offset distances (Δh).

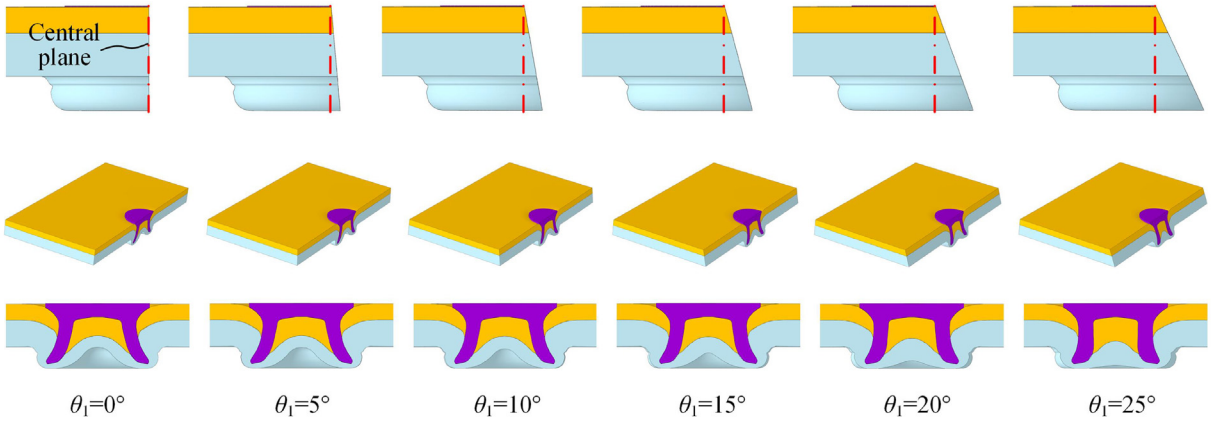

Fig. 8. Joint appearances and cross-sectional profiles at different pure rotation angles (θ_1).

sectional profile. The joint appearances and cross-sectional profiles at such type of cutting positions would be a combination of Figs. 7 and 8, and are not presented here to avoid repetition.

3. Evaluation of cutting position's effects on the joint quality indicators

To better understand the relationships between the cutting position and the measurement errors of the joint quality indicators, influences of the three types of improper cutting positions on the rivet head height (H_1), the interlock (I) and the remaining bottom sheet thickness were analysed and discussed.

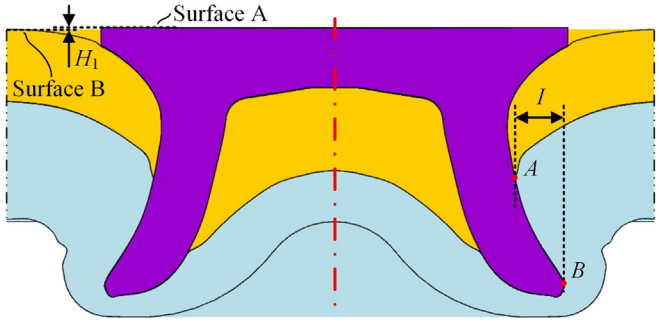

Fig. 9. Locations of the two boundaries for the rivet head height (H_1) and the two boundaries for the interlock (I).

3.1. Error estimation of the rivet head height (H_1)

As shown in Fig. 9, the rivet head height (H_1) is the vertical distance between the top surface of the rivet (Surface A) and the upper surface of the top sheet (Surface B). During the experimental tests, the locations of these two surfaces are not affected by the cutting position. Therefore, the H_1 observed on the cutting plane equals exactly to the true H_1 on the joint central plane, and will not be influenced by the Δh and θ_1.

3.2. Error estimation of the interlock (I)

According to the definition, the magnitude of I is directly determined by the locations of the inner interlock boundary (Point A) and the outer interlock boundary (Point B), as shown in Fig. 9. The appearance of the Δh and θ_1 would affect the measured value of I by altering the locations of the two interlock boundaries. Therefore, influences of the three types of improper cutting positions on the I were analysed, and the corresponding relative and absolute errors of interlock were estimated.

3.2.1. With only the offset distance (Δh)

As shown in Fig. 10, the inner and outer interlock boundaries are two circles in the three-dimensional space (Circle A for the inner boundary and Circle B for the outer boundary). The intersection points (i.e. Points A and B) between the two circles and the joint central plane are the true

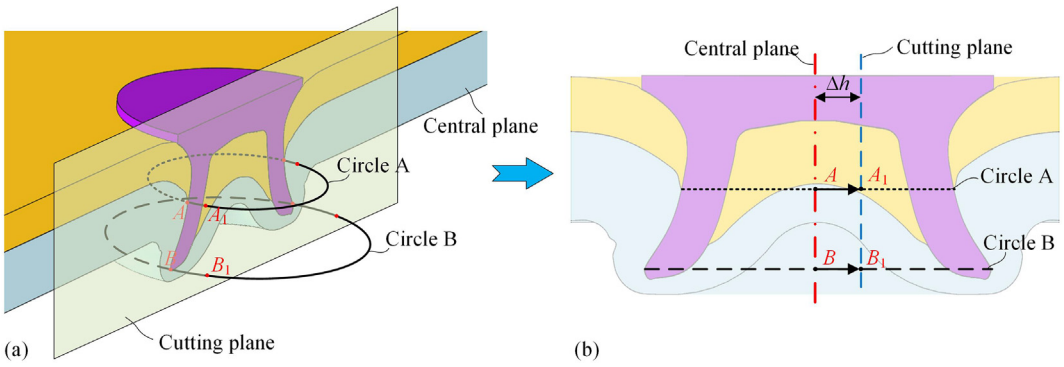

Fig. 10. Projections of the two interlock boundaries on the cutting plane with an offset distance (Δh).

positions of the two interlock boundaries. When there is a Δh between the joint central plane and the cutting plane, the observed positions of the two interlock boundaries become the intersection points between the two circles and the cutting plane (Point A_1 and B_1). The true interlock boundaries on the central plane are projected onto the cutting plane along the trajectories of the Circle A and B.

To evaluate the interlock error induced by the improper cutting position, as shown in Fig. 11, the measured interlock (I_m) on the cutting plane was firstly derived using the dimensions on the joint central plane and the cutting plane. The $R_{in\text{-}true}$ and I_{true} denote the true radius of the inner interlock boundary and the true interlock on the joint central plane. The magnitude of $R_{in\text{-}true}$ is determined by the initial radius of rivet shank and its degree of deformation during the riveting process [7]. According to the geomatical relationships, the I_m can be expressed as a function of the I_{true}, $R_{in\text{-}true}$ and Δh:

$$I_m = \sqrt{(R_{in-true} + I_{true})^2 - \Delta h^2} - \sqrt{R_{in-true}{}^2 - \Delta h^2} \tag{1}$$

The relative error (δ_{offset}) and absolute error (e_{offset}) of interlock with only the Δh can be calculated using Eqs. (2) and (3) respectively. Substituting Eq. (1) into Eqs. (2) and (3) yields Eqs. (4) and (5). By observing the structures of Eqs. (4) and (5), it can be found that the δ_{offset} and e_{offset} are always equal to ($\Delta h = 0$) or greater than zero ($\Delta h > 0$). This means the I_m would be always greater than the I_{true} due to the existence of Δh. Meanwhile, it was found that the magnitudes of δ_{offset} and e_{offset} are not only affected by the Δh but also by the $R_{in\text{-}true}$ and I_{true}.

$$\delta_{offset} = \frac{I_m - I_{true}}{I_{true}} \times 100\% \tag{2}$$

$$e_{offset} = I_m - I_{true} \tag{3}$$

$$\delta_{offset} = \left(\frac{I_{true} + 2R_{in-true}}{\sqrt{(R_{in-true} + I_{true})^2 - \Delta h^2} + \sqrt{R_{in-true}^2 - \Delta h^2}} - 1 \right) \times 100\% \tag{4}$$

$$e_{offset} = \sqrt{R_{in-true}^2 + I_{true}^2 - \Delta h^2 + 2 \cdot I_{true} \cdot R_{in-true}} - \sqrt{R_{in-true}^2 + I_{true}^2 - \Delta h^2 + 2 \cdot I_{true} \cdot \sqrt{R_{in-ture}^2 - \Delta h^2}} \tag{5}$$

Taking the SPR joints with ∅5.3 mm boron steel rivet and AA5754 sheets as an example, the influences of the Δh on the interlock were demonstrated. According to the experimental results reported in [26,27], for this type SPR joints, the $R_{in\text{-}true}$ usually locates in the range of 2.65 mm–4.0 mm and the I_{true} generally belongs to the range of 0.0 mm–2.0 mm. Using Eqs. (4) and (5), surface diagrams of the e_{offset} and δ_{offset} at the offset distances 0.5 mm, 1.0 mm, 1.5 mm, 2.0 mm and 2.5 mm are presented Figs. 12 and 13 respectively. It can be seen that both of the e_{offset} and δ_{offset} showed an increasing tendency with the increment of Δh. For a fixed Δh, the e_{offset} showed an increasing trend with the increment of I_{true}. In contrast, the δ_{offset} demonstrated an opposite trend and decreased with the increment of I_{true}. Moreover, both of the

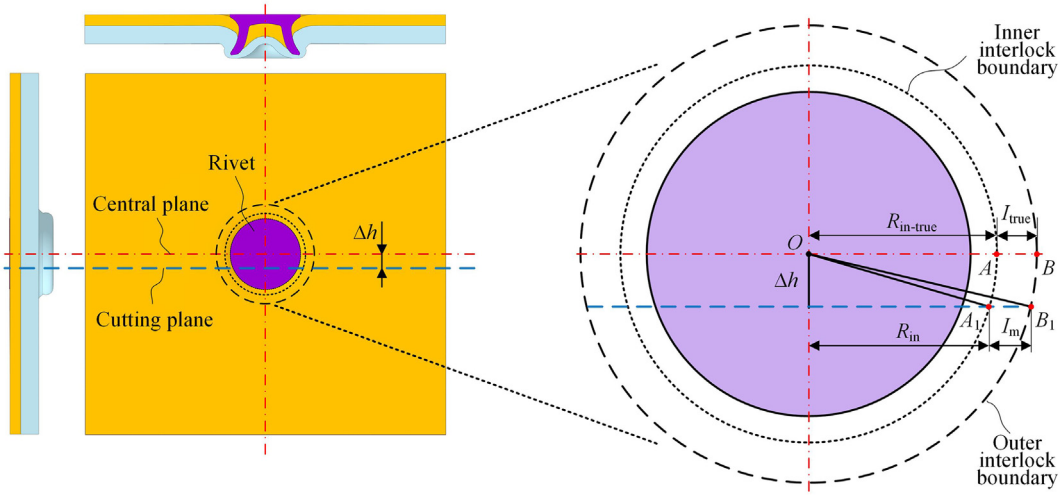

Fig. 11. Schematic of the interlock values on the joint central plane and on the cutting plane with an offset distance (Δh).

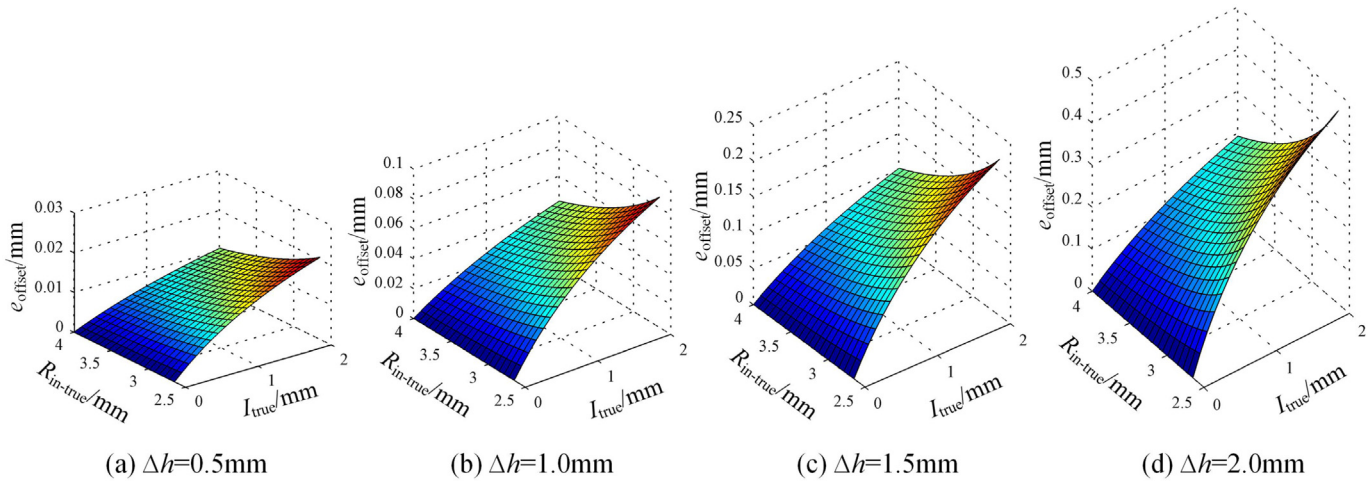

Fig. 12. Absolute error (*e*offset) of interlock with different offset distances (Δ*h*).

e_{offset} and δ_{offset} showed a decreasing tendency with the increment of $R_{in\text{-}true}$. This means that the Δ*h* would impose a smaller influence on the measurement accuracy of interlock if the interlock was formed at a position far from the joint axis. As shown in Fig. 12, the $R_{in\text{-}true}$ showed very limited influence on the e_{offset} when the interlock was relatively small (I_{true} < 0.5 mm), but an obvious impact when the interlock had a large value (I_{true} > 1.0 mm). As shown in Fig. 13, the $R_{in\text{-}true}$ always had a significant influence on the δ_{offset}, and imposed a greater influence with a small interlock than with a large one. In addition, it can also be found that both of the e_{offset} and δ_{offset} could still maintain at a low level when the Δ*h* increased to 1.0 mm as shown in Figs. 12(b) and 13(b). However, further increment of Δh resulted in unacceptable measurement errors as presented in Figs. 12(c),(d) and 13(c),(d).

3.2.2. With only the rotation angle (θ_1)

As shown in Fig. 14, the joint central plane and the cutting plane become not parallel when there is a rotation angle (θ_1). The two interlock boundaries on the joint central plane (Points *A* and *B*) are projected along the trajectories of Circle A and B onto two different planes (Plane A and Plane B) paralleling to the central plane. The Δh_1 denotes the offset distance from the Plane A to the central plane, and can be expressed as a function of the θ_1 and the vertical distance (S_1) between the inner interlock boundary (Point *A*) and the top surface of the rivet, as shown in Eq. (6). The Δh_2 denotes the offset distance between the plane A and plane B. It can be expressed as a function of the θ_1 and the vertical distance (S_2) between the two interlock boundaries (Points *A* and *B*), as shown in Eq. (7).

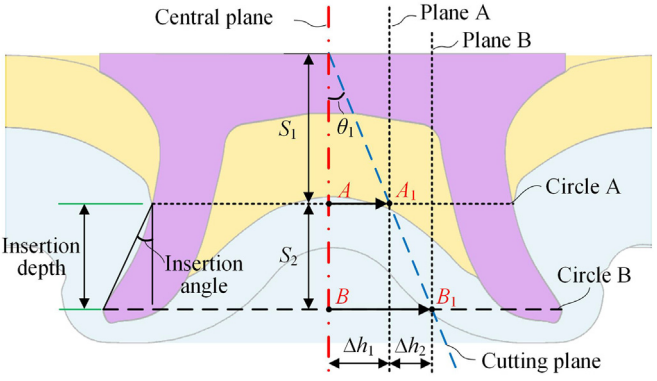

Fig. 14. Projections of the two interlock boundaries from the joint central plane to the cutting plane with a rotation angle (θ_1).

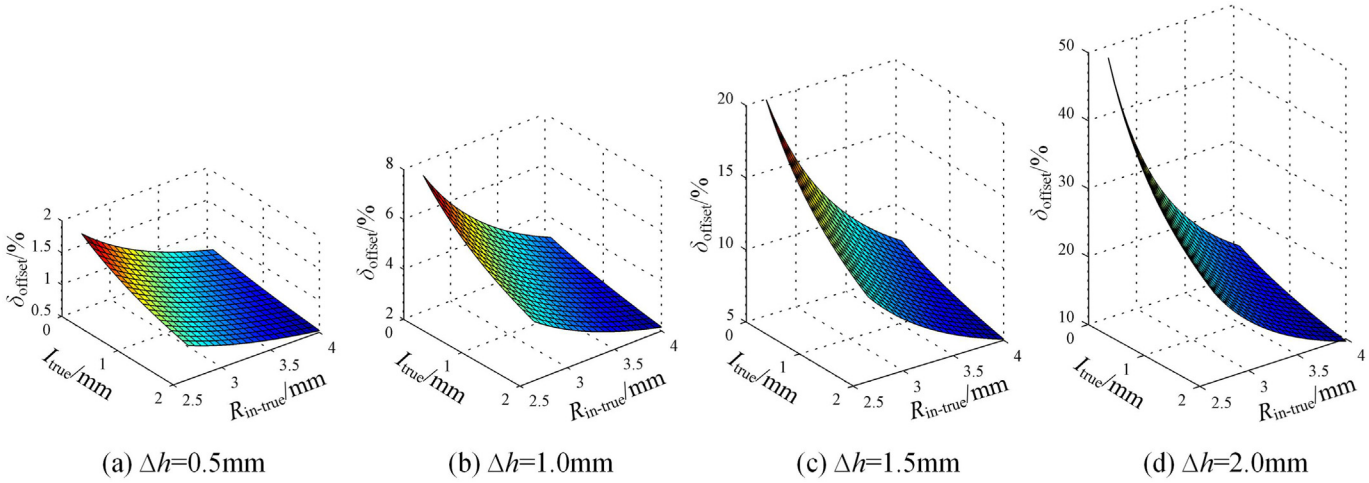

Fig. 13. Relative error (δ_{offset}) of interlock with different offset distances (Δ*h*).

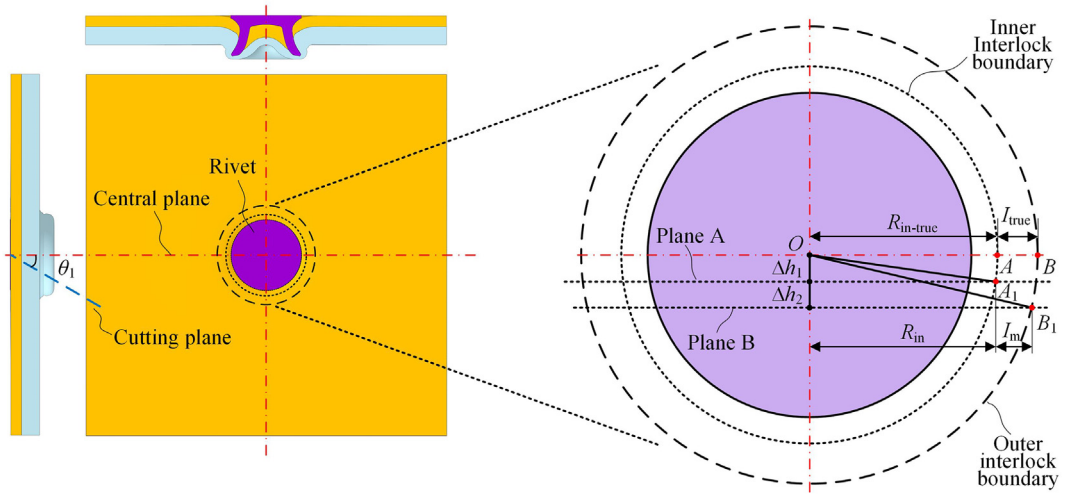

Fig. 15. Schematic of the interlock values on the joint central plane and the cutting plane with a rotation angle (θ_1).

$$\Delta h_1 = S_1 \cdot \tan\theta_1 \tag{6}$$

$$\Delta h_2 = S_2 \cdot \tan\theta_1 \tag{7}$$

Fig. 15 shows the dimensions on the joint central plane and on the cutting plane. According to the geometrical relationships, the I_m can be expressed as a function of the $R_{in\text{-}true}$, I_{true}, Δh_1 and Δh_2, as shown in Eq. (8). Substituting Eqs. (6) and (7) into (8) gives Eq. (9). It can be seen that the I_m is not only affected by the horizontal distance from the interlock formation zone to the joint axis (i.e. $R_{in\text{-}true}$), but also influenced by the vertical distance from the interlock formation zone to the rivet head (i.e. S_1 and S_2). To evaluate the effects of the θ_1 on the interlock measurement accuracy, the relative error ($\delta_{rotation}$) and absolute error ($e_{rotation}$) of the interlock with only the θ_1 are calculated using Eqs. (10) and (11) respectively. Substituting Eq. (9) into Eqs. (10) and (11) yields Eqs. (12) and (13). However, different from the δ_{offset} and e_{offset}, the sign of the $\delta_{rotation}$ and $e_{rotation}$ cannot be determined by simply comparing the structures of Eqs. (12) and (13).

$$I_m = \sqrt{(R_{in-true} + I_{true})^2 - (\Delta h_1 + \Delta h_2)^2} - \sqrt{R_{in-ture}^2 - \Delta h_1^2} \tag{8}$$

$$I_m = \sqrt{(R_{in-true} + I_{true})^2 - (S_1 + S_2)^2 \cdot \tan\theta_1{}^2} - \sqrt{R_{in-true}{}^2 - S_1^2 \cdot \tan\theta_1{}^2} \tag{9}$$

$$\delta_{rotation} = \frac{I_m - I_{true}}{I_{true}} \times 100\% \tag{10}$$

$$e_{rotation} = I_m - I_{true} \tag{11}$$

$$\delta_{rotation} = \left(\frac{I_{true} \cdot (2R_{in-true} + I_{true}) - S_2{}^2 \cdot \tan\theta_1{}^2}{I_{true} \cdot \left(\sqrt{(R_{in-true} + I_{true})^2 - (S_1 + S_2)^2 \cdot \tan\theta_1{}^2} + \sqrt{R_{in-true}{}^2 - S_1^2 \cdot \tan\theta_1{}^2} \right)} - 1 \right) \times 100\% \tag{12}$$

$$e_{rotation} = \frac{I_{true} \cdot (2R_{in-true} + I_{true}) - S_2{}^2 \cdot \tan\theta_1{}^2}{\sqrt{(R_{in-true} + I_{true})^2 - (S_1 + S_2)^2 \cdot \tan\theta_1{}^2} + \sqrt{R_{in-true}{}^2 - S_1^2 \cdot \tan\theta_1{}^2}} - I_{true} \tag{13}$$

To find out the effects of the θ_1 on the interlock, the $e_{rotation}$ and $\delta_{rotation}$ at different rotation angles (5°, 10°, 15° and 20°) of SPR joints with the ∅5.3 mm boron steel rivet and AA5754 sheets were plotted in Figs. 16 and 17. The $R_{in\text{-}true}$ and S_1 were assumed to be fixed at 2.65 mm and 3.0 mm respectively. This would not affect the changing

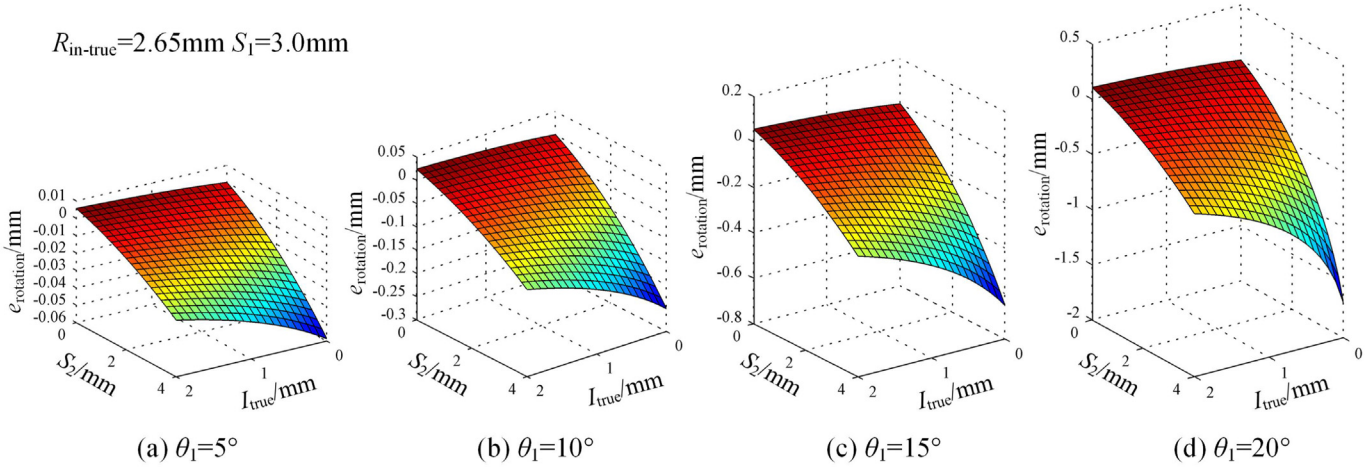

Fig. 16. Absolute error (erotation) of interlock with different rotation angles (θ_1).

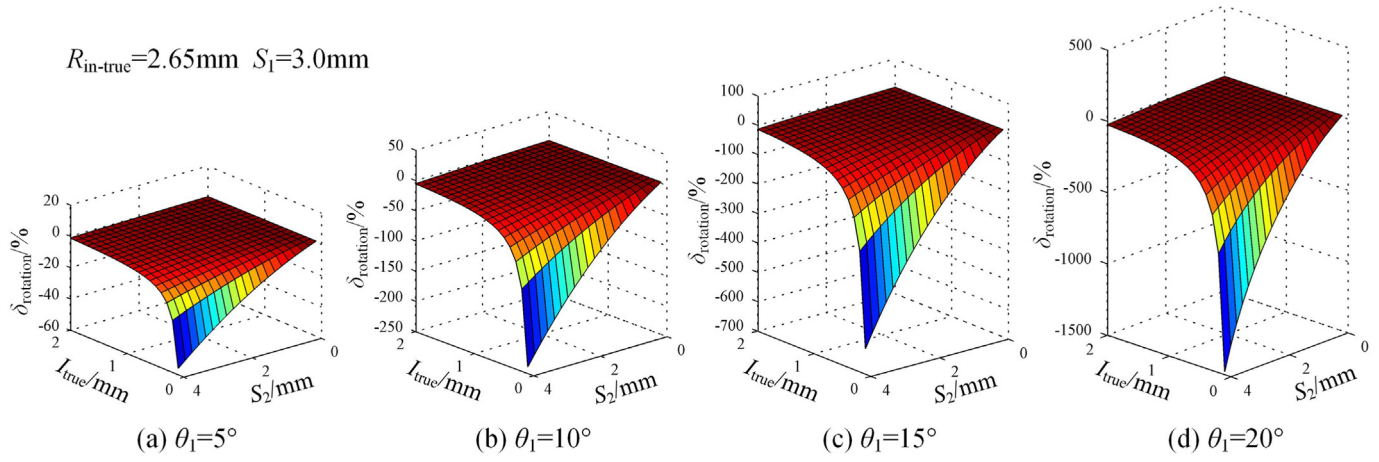

Fig. 17. Relative error ($\delta_{rotation}$) of interlock with different rotation angles (θ_1).

trend of interlock with varying rotation angles. The I_{true} and the S_2 changed within the ranges of 0.0 mm–2.0 mm and 0.0 mm–4.0 mm. It can be seen from Fig. 16 that the $e_{rotation}$ was negative in most cases and only had a positive value when the S_2 was very close to zero. This indicates that the I_m is more likely smaller than the I_{true} if only the θ_1 existed between the joint central plane and the cutting plane. For a fixed I_{true}, the absolute value of $e_{rotation}$ always demonstrated an increasing trend with the increment of S_2. This means the interlock formed by a larger insertion angle would be less affected by the θ_1 compared with that formed by a larger insertion depth (Fig. 14). For a fixed S_2, the absolute value of $e_{rotationv}$ always showed a decreasing trend with the increment of I_{true}. A faster changing speed of $e_{rotationv}$ was found with a larger S_2. As shown in Fig. 17, similar changing trends of $\delta_{rotation}$ were observed with the variations of S_2 and I_{true}. It is worth noting that the largest absolute value of $\delta_{rotation}$ was found at a small I_{true} but a large S_2.

3.2.3. With the offset distance (Δh) and rotation angle (θ_1)

In practical applications, the cutting offset and the cutting rotation more likely occur at the same time. According to the rotation directions of the cutting plane, there are two possible situations as shown in Fig. 18 (a) with a positive rotation angle ($\theta_1 > 0$) and in Fig. 18(b) with a negative rotation angle ($\theta_1 < 0$). The projected two interlock boundaries (Points A_1 and B_1) move far away from the joint central plane when the θ_1 is positive, while move close to the joint central plane with a negative θ_1. Fig. 19 shows the relationships between the I_{true} and the I_m at the two situations. According to the geometrical relationships, the I_m can be calculated using Eq. (14) for the $\theta_1 > 0$ and Eq. (15) for the $\theta_1 < 0$. The Δh_1 and Δh_2 can be calculated with Eq. (16). Substituting Eq. (16) into Eqs. (14) and (15) yield a same equation Eq. (17). So the I_m under the two situations can be calculated using a uniform equation. The relative error ($\delta_{off+rot}$) and absolute error ($e_{off+rot}$) of interlock with Δh as well as θ_1 can be calculated using Eqs. (18) and (19) respectively. The sign of $\delta_{off+rot}$ and $e_{off+rot}$ will be positive if the Δh had a dominating effect and be negative if the θ_1 had a greater influence. Due to the multiple variables involved in Eq. (17), it is difficult to discuss the changing trends of the $\delta_{off+rot}$ and $e_{off+rot}$. Instead, the interaction effects of Δh and θ_1 on the measurement accuracy of interlock were discussed in the following sections using experimental SPR joint data.

$$I_m = \sqrt{(R_{in-true} + I_{true})^2 - (\Delta h + \Delta h_1 + \Delta h_2)^2} - \sqrt{R_{in-true}{}^2 - (\Delta h + \Delta h_1)^2} \tag{14}$$

$$I_m = \sqrt{(R_{in-true} + I_{true})^2 - (\Delta h - \Delta h_1 - \Delta h_2)^2} - \sqrt{R_{in-true}{}^2 - (\Delta h - \Delta h_1)^2} \tag{15}$$

$$\begin{cases} \Delta h_1 = S_1 \cdot \tan\theta_1 \\ \Delta h_2 = S_2 \cdot \tan\theta_1 \end{cases} \quad (\theta_1 > 0) \qquad \begin{cases} \Delta h_1 = -S_1 \cdot \tan\theta_1 \\ \Delta h_2 = -S_2 \cdot \tan\theta_1 \end{cases} \quad (\theta_1 < 0) \tag{16}$$

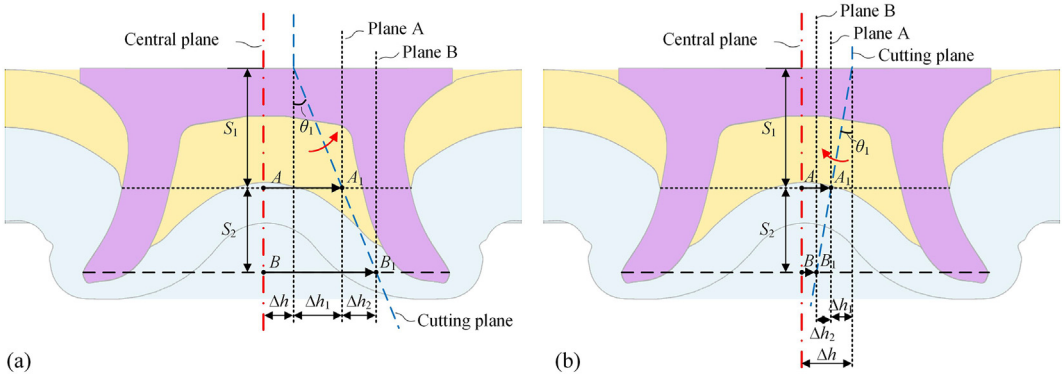

Fig. 18. Projections of the two interlock boundaries from the joint central plane to the cutting plane with a offset distance (Δh) and a rotation angle (θ_1): (a) $\theta_1 > 0$ and (b) $\theta_1 < 0$.

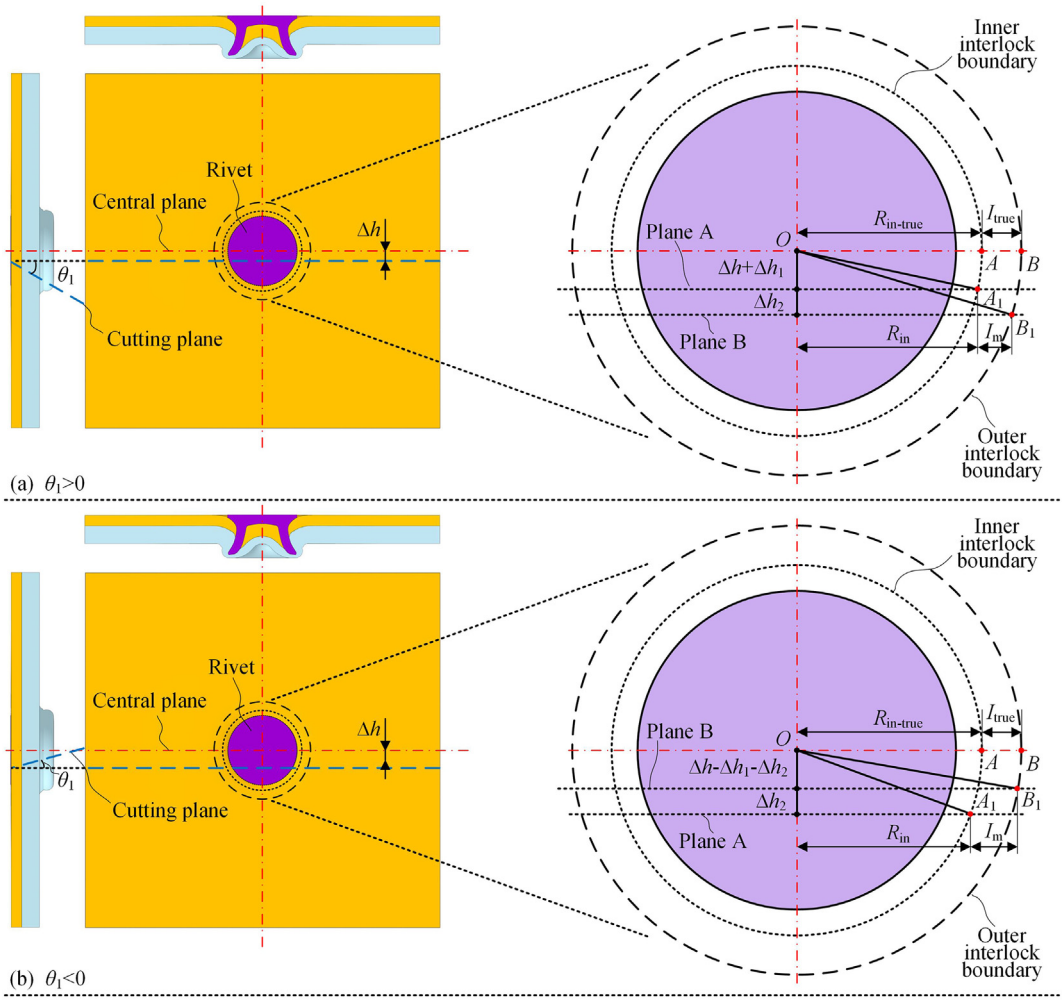

Fig. 19. Schematics of the interlock on the joint central plane and on the measurement plane with a offset distance (Δh) and a rotation angle (θ_1).

$$I_m = \sqrt{(R_{in-true} + I_{true})^2 - (\Delta h + S_1 \cdot \tan\theta_1 + S_2 \cdot \tan\theta_1)^2} - \sqrt{{R_{in-true}}^2 - (\Delta h + S_1 \cdot \tan\theta_1)^2} \quad (17)$$

$$\delta_{off+rot} = \frac{I_m - I_{true}}{I_{true}} \times 100\% \quad (18)$$

$$e_{off+rot} = I_m - I_{true} \quad (19)$$

3.3. Error estimation of the remaining bottom sheet thickness

As shown in Fig. 20(a), the remaining bottom sheet thickness on the joint cross-sectional profile is directly determined by the infinite points on the upper surface (Red) and lower surface (Black) of the bottom sheet. The projection of these points from the joint central plane to the cutting plane is very similar to that of the two interlock boundary points in Fig. 10. Taking the points *A* and *B* in Fig. 20(a) as an example, the projection trajectories (Circles A and B) of the two points are shown in Fig. 20(b). When with the Δh or θ_1, only part of these points

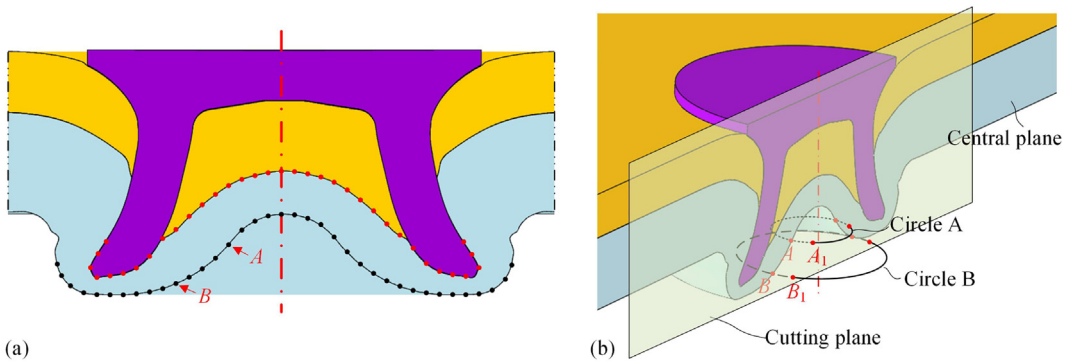

Fig. 20. Schematics of (a) Points located on the upper and lower surfaces of the bottom sheet and (b) Projection of the boundary points *A* and *B* from the joint central plane to the cutting plane.

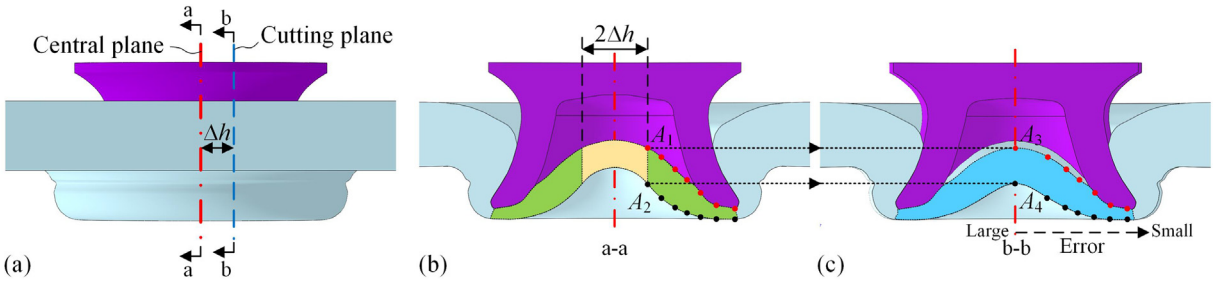

Fig. 21. Schematic of the (a) Ideal and actual cutting positions, (b) the bottom sheet profile on the joint central plane and (c) the bottom sheet profile on the cutting plane with an offset distance (Δh).

can be projected from the joint central plane to the cutting plane. Meanwhile, the relative positions of these points would be affected during the projection process, and become different from the original ones on the joint central plane. This would lead to an unrealistic bottom sheet thickness distribution. Therefore, influences of the three types of improper cutting positions on the captured bottom sheet profile were analysed and discussed qualitatively.

3.3.1. With only the offset distance (Δh)

Fig. 21 shows the true bottom sheet profile on the joint central plane and the captured one on the cutting plane with the Δh. It can be seen that only the bottom sheet profile in the green region of Fig. 21 (b) was projected onto the cutting plane as shown in Fig. 21(c). The bottom sheet profile in the yellow region of Fig. 21(b) could not be projected onto the cutting plane and thus the thickness data in this region was not accessible on the cutting plane. The width of the yellow region is two times of the Δh, which means the amount of missing thickness data increase with the increment of the Δh.

It can also be found that the shape of the green region in Fig. 21 (b) is quite different from that of the blue region in Fig. 21(c). During the projection process, the green region was stretched along the horizontal direction in order to cover the larger blue region. Fig. 22 shows the projection trajectories of these boundary points from the green region to the blue region. The radius of the projection trajectory is different for each point and equals to the distance from the projected point to the original point *O*. Due to the different trajectory radiuses, a large distortion occurred around the joint central region while a limited distortion was found around the rivet tip. For example, the green region between points A_1 and B_1 was stretched to a wider blue region between the points A_3 and B_3. While the green region between points D_1 and E_1 was stretched to an almost same width blue region between the points D_3 and E_3. According to the projection pattern, the bottom sheet thickness along the vertical direction in the green region of Fig. 21(b) can be exactly measured on the cutting plane but with a position shift ($\leq \Delta h$). While the measured thickness along the direction perpendicular to the bottom sheet surface would be greater than the true values in the green region. Because of the different distortion levels on the blue region, the bottom sheet thickness measured around the joint central area would have a higher measurement error than that measured around the rivet tip. In other words, the measurement error of bottom sheet thickness demonstrates a decreasing trend from the joint centre to the rivet tip, as presented in Fig. 21(c).

Taking the SPR joint with the 1.2 mm + 2.0 mm AA5754 sheets and the 6.0 mm long boron steel rivet as an example, the virtually captured bottom sheet profiles with offset distances 0.0 mm, 0.5 mm, 1.0 mm and 1.5 mm are compared in Fig. 23. It can be seen that the Δh showed very limited influences on the bottom sheet profile when the Δh had a small value (e.g. 0.5 mm), as shown in Fig. 23(a). The captured bottom sheet profile with $\Delta h = 0.5$ mm was still very close to that from the joint central plane ($\Delta h = 0.0$ mm). So the measurement error of bottom sheet thickness would maintain at a very low level. However, when the Δh increased to larger values (e.g. 1.0 mm and 1.5 mm), as shown in Fig. 23 (b), the inspected bottom sheet profiles became quite different from that on the joint central plane, especially around joint central area. Because of the high-level measurement error, the real quality of the

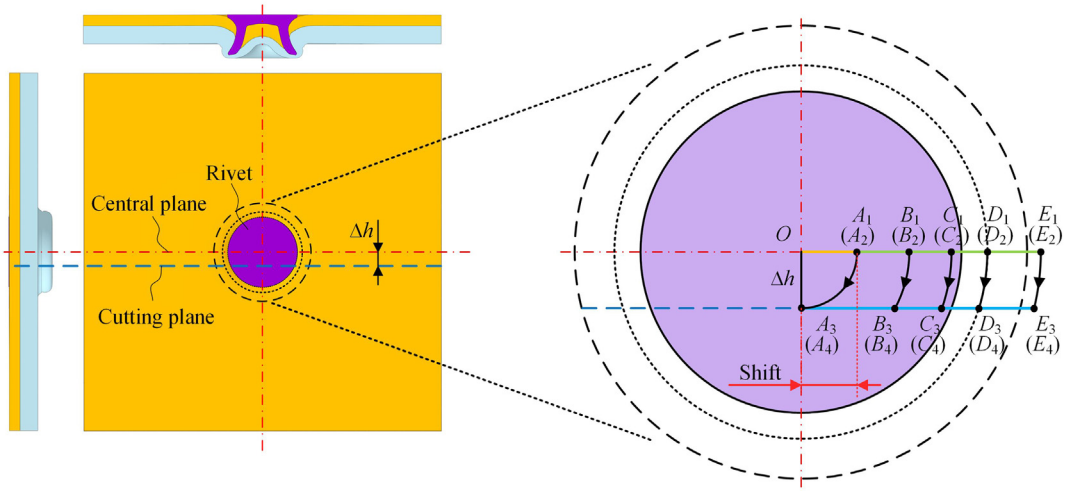

Fig. 22. Projection trajectories of the boundary points from the joint central plane to the cutting plane with an offset distance (Δh).

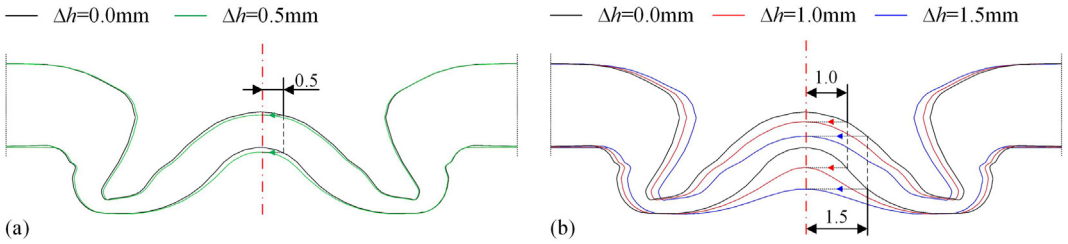

Fig. 23. Virtually captured bottom sheet profiles on the cutting plane with different offset distances (Δh): (a) 0.0 mm and 0.5 mm, and (b) 0.0 mm, 1.0 mm and 1.5 mm.

deformed bottom sheet could not be reflected by the measured bottom sheet thickness on the cutting plane. Therefore, it is necessary to control the Δh within a small range in order to accurately evaluate the quality of the deformed bottom sheet.

3.3.2. With only the rotation angle (θ_1)

Fig. 24 shows the captured bottom sheet profiles on the joint central plane and on the cutting plane with the θ_1. Similar to the Δh, the θ_1 would also lead to thickness data missing of the bottom sheet as well as distorted bottom sheet profile on the cutting plane. As presented in Fig. 24(b), the width of this thickness data missing region (Yellow region) is determined not only by the θ_1 but also the relative distance between the rivet head and the bottom sheet. Increments of the θ_1 or the relative distance could result in more missing data of the bottom sheet thickness. Only the green region in Fig. 24(b) was projected to the blue region in Fig. 24(c) on the cutting plane. Fig. 25 shows the projection trajectories of these boundary points from the green region to the blue region. Due to the existence of θ_1, the boundary points on the green region were projected to different planes paralleling to the joint central plane. Different from with only the Δh, it can be seen that the boundary points located on the same vertical line in the green region (e.g. points B_1 and B_2) were projected to different vertical lines (e.g. points B_3 and B_4). As a result, the measured bottom sheet thickness along the vertical direction on the cutting plane in Fig. 24(c) would be slightly larger than the true value on the joint central plane shown in Fig. 24(b). The measured bottom sheet thickness along the direction perpendicular to the bottom sheet surface would be more likely larger than the true value.

Taking the SPR joint with 1.2 mm + 2.0 mm AA5754 sheets and 6.0 mm long boron steel rivet as an example, the virtually captured bottom sheet profiles with rotation angles 0°, 5°, 10°, 15° and 20° are compared in Fig. 26. As shown in Fig. 26(a), the captured bottom sheet profile on the cutting plane with $\theta_1 = 5°$ was almost the same with that on the joint central plane ($\theta_1 = 0°$). However, obviously different bottom sheet profiles were observed when the θ_1 increased to larger values (i.e. 10°, 15° and 20°) as shown in Fig. 26(b). It can be seen that the θ_1 imposed a larger influence on the lower boundary (Zone1) than the upper boundary (Zone2) of the bottom sheet. Therefore, it is very important to control the θ_1 within a small range to accurately evaluate the quality of the deformed bottom sheet.

3.3.3. With the offset distance (Δh) and rotation angle (θ_1)

When the cutting offset and the cutting rotation occurred at the same time, the effects of the Δh and θ_1 would be superimposed to affect the bottom sheet profile. It is worth noting that the rotation direction of the cutting plane would impose different influences on the bottom sheet profile, as shown in Fig. 27. When with a positive rotation angle ($\theta_1 > 0$), a larger part of the bottom sheet profile (Yellow region) on the joint central plane cannot be projected onto the cutting plane as presented in Fig. 27(a). This would lead to a larger measurement error of bottom sheet thickness than with only a Δh or only a θ_1. In contrast, when with a negative rotation angle ($\theta_1 < 0$) as presented in Fig. 27(b), the missing thickness data caused by the Δh would reduce to a smaller amount (Yellow region). This effectively reduces the distortion degree of the captured bottom sheet profile and improves the measurement accuracy of bottom sheet thickness. Previously, the bottom sheet profiles of SPR joint with AA5754 sheets and 6.0 mm long rivet with varying Δh and θ_1 have been compared in Figs. 23 and 26 respectively. With both of the Δh and θ_1, the captured bottom sheet profile would be determined by the relative magnitudes of the Δh and θ_1. Due to the plentiful combinations of the Δh and θ_1, the bottom sheet profiles of this SPR joint at different cutting positions were not presented here.

As discussed above, the appearances of the Δh and θ_1 would affect the captured bottom sheet profile on the cutting plane. As a result, the measurement accuracy of the T_{min} would be inevitably influenced. Depending on the formation position, the measured T_{min} may have different error levels. If the T_{min} was formed around the joint central area, it may have a very large error because of the missing thickness data (Yellow region in Fig. 27) and the large bottom sheet profile distortion around the joint central area. In contrast, if the T_{min} was formed around the rivet tip, it more likely has a limited error due to the minor distortion of the bottom sheet profile around the rivet tip.

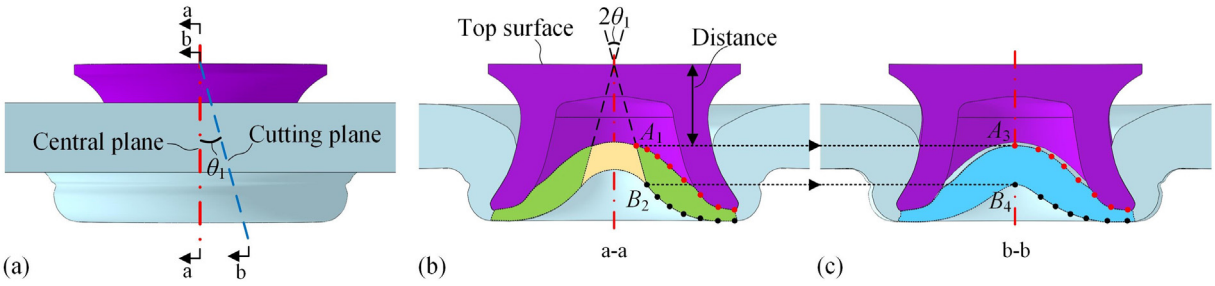

Fig. 24. Schematic of the (a) Ideal and actual cutting positions, (b) the bottom sheet profile on the joint central plane and (c) the bottom sheet profile on the cutting plane with a rotation angle (θ_1).

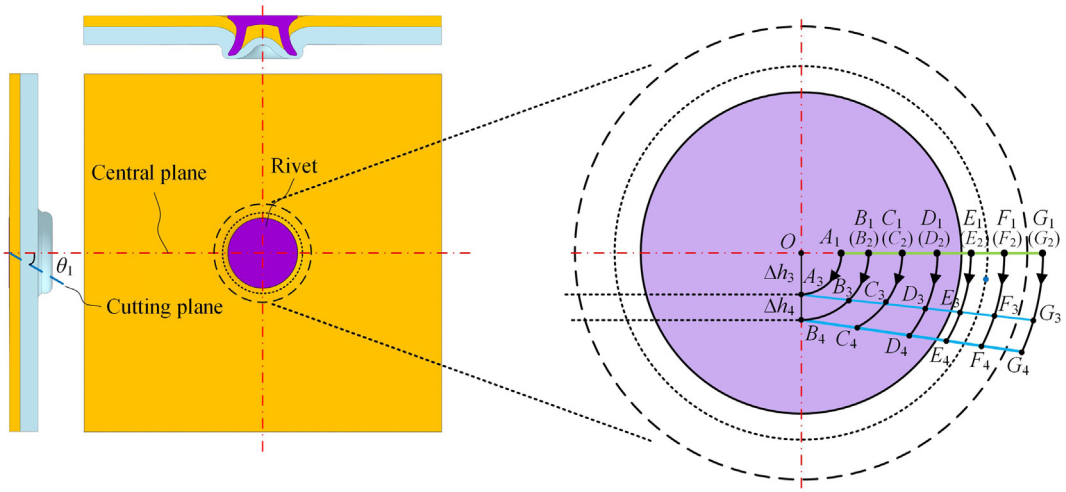

Fig. 25. Projection trajectories of the boundary points from the joint central plane to the cutting plane with a rotation angle (θ_1).

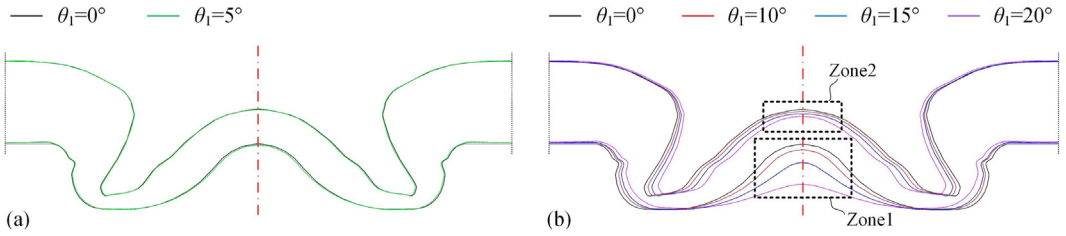

Fig. 26. Virtually captured bottom sheet profiles on the cutting plane with different rotation angles (θ_1): (a) 0° and 5°, and (b) 0°, 10°, 15°, 20°.

4. Correction of cutting position's effects on the joint quality indicators

Under the conditions when the SPR joints were not or could not be sectioned through the joint centre plane (e.g. Joints cut from the car BIW), it is important and necessary to correct/compensate the errors of joint quality indicators induced by the improper cutting position. As previously discussed, the rivet head height (H_1) is not affected by the cutting position and thus does not need any correction. In addition, because the bottom sheet profile is determined by an infinite number of points on the upper and lower surfaces of the deformed bottom sheet, it is very difficult to correct the error of the remaining bottom sheet

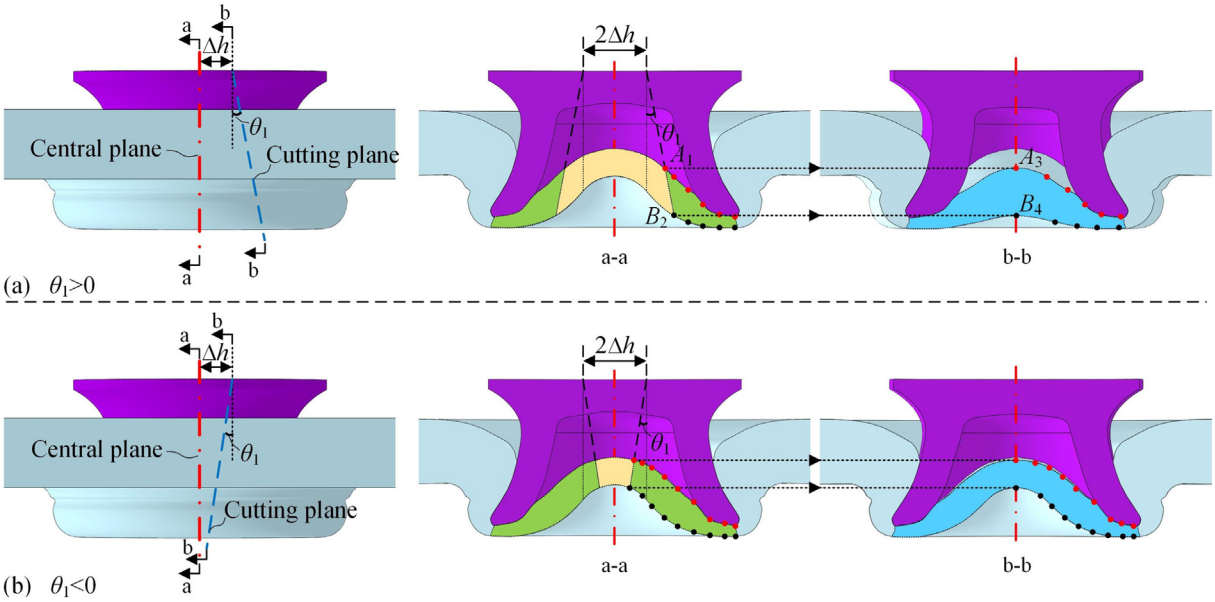

Fig. 27. Schematic of the bottom sheet profiles on the joint central plane and on the cutting plane with an offset distance (Δh) and a rotation angle (θ_1).

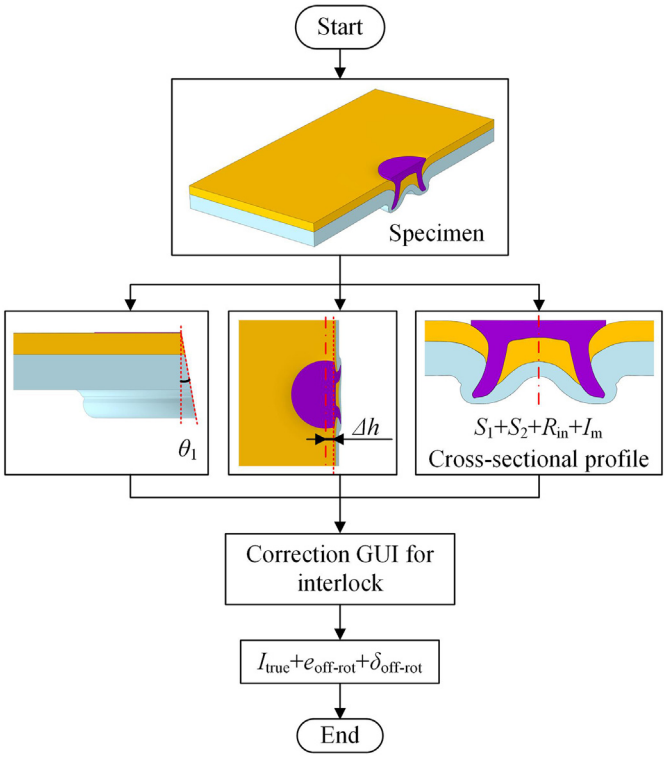

Fig. 28. Flow chart for the interlock error correction in practical applications.

thickness. First of all, the missing thickness data in the yellow region of the joint central plane (as shown in Fig. 27) cannot be recovered from the captured joint profile on the cutting plane; Secondly, it is possible but requires a huge workload to eliminate the distortion of the captured bottom sheet profile from the cutting plane. Therefore, the correction of the bottom sheet thickness was not discussed in this study.

For the interlock, its value is only determined by the positions of the inner and outer interlock boundaries. Therefore, it is relatively easy to correct the interlock error induced by the improper cutting position. According to the geometrical relationships shown in Fig. 19, the I_{true} can be expressed as a function of six dimensions measured on the sectioned joint specimen, as shown in Eq. (20). The similar strategy was also utilized by Gerstmann and Awiszus [25] to compensate the interlock error caused by the improper cutting position of flat-clinch joints, but only the offset distance was considered in their study. The R_{in} is the measured radius of the inner interlock boundary on the cutting plane. Fig. 28 shows the procedures to correct the interlock error in practical applications: First, the Δh and θ_1 were measured from the sectioned specimen; Then, the joint cross-sectional profile was captured, and the S_1, S_2, R_{in} and I_m were measured; Finally, all the six measured parameters were entered into Eq. (20) to calculate the I_{true}.

$$I_{true} = \sqrt{(R_{in}+I_m)^2+(\Delta h+S_1\cdot\ \tan\theta_1+S_2\cdot\ \tan\theta_1)^2} - \sqrt{{R_{in}}^2+(\Delta h+S_1\cdot\ \tan\theta_1)^2} \quad (20)$$

In practical applications, measurement of the six parameters (i.e. Δh, θ_1, S_1, S_2, R_{in} and I_m) is very critical for the correction result of interlock. There are two ways to get the value of Δh: (1) Directly measure the diameter of the rivet head (D_h) and the remaining rivet head thickness perpendicular to the sectioned surface (l_1) on the specimen as shown in Fig. 29(a), and then calculate the Δh using Eq. (21); (2) Measure the diameter of the rivet head (D_h) and the width of the rivet head ($D_{h\text{-}m}$) on the captured joint cross-sectional profile as presented in Fig. 29(b), and then calculate the Δh using Eq. (22). Similarly, there are also two approaches to obtain the θ_1: (1) Directly measure the included angle (α) between the top surface of rivet head and the joint sectioned surface as shown in Fig. 29(c), and then calculate the θ_1 using Eq. (23); (2) Measure the height of the captured joint cross-sectional profile from direction A (l_2) and the height of the captured joint cross-sectional profile from the direction B (l_3) as shown in Fig. 29(d), and then calculate the θ_1 using Eq. (24).

$$\Delta h = l_1 - \frac{D_h}{2} \quad (21)$$

$$\Delta h = \frac{1}{2}\sqrt{{D_h}^2+{D_{h-m}}^2} \quad (22)$$

$$\theta_1 = \alpha - \frac{\pi}{2} \quad (23)$$

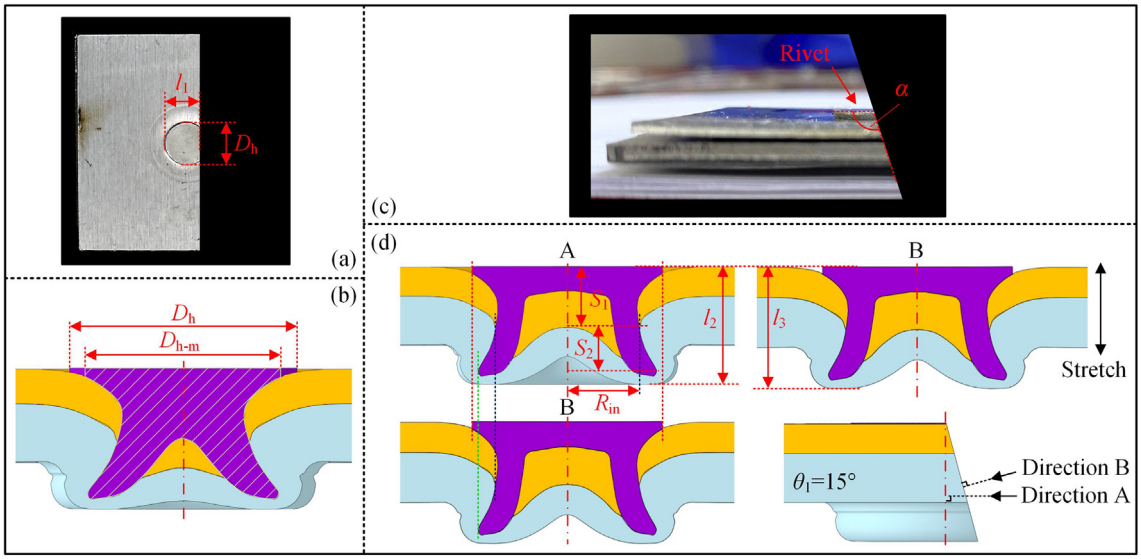

Fig. 29. Strategies to obtain the six parameters (Δh, θ_1, S_1, S_2, R_{in} and I_m) for the interlock error correction.

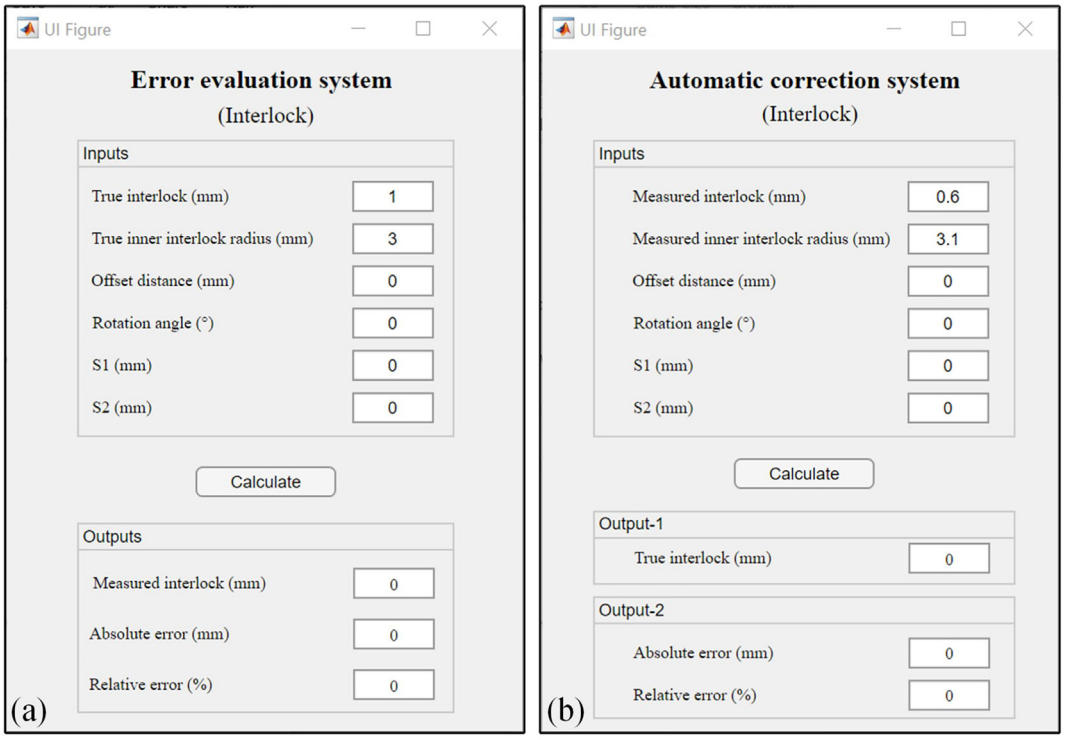

Fig. 30. Developed graphical user interfaces (GUI) for (a) Interlock error estimation and (b) Interlock error correction.

Table 1
Joint configurations and experiment results.

Joint no.	Thickness (mm)		Rivet (Boron steel)	Die	Experiment results			
	Top sheet/T_t (AA5754)	Bottom sheet/T_b (AA5754)			S_1 (mm)	S_2 (mm)	$R_{in\text{-}true}$ (mm)	I_{true} (mm)
1-1	1.2	1.0	C5.3*5.0	Pip die	2.60	0.71	3.47	0.45
1-2	1.2	1.2	(280 ± 30HV10)		2.60	0.87	3.18	0.50
1-3	1.2	1.5			2.72	0.97	3.11	0.54
1-4	1.2	2.0			2.54	1.24	2.86	0.66
1-5	1.0	1.5			2.34	1.16	2.99	0.61
1-6	1.5	1.5			2.95	0.86	3.19	0.42
2-1	1.5	1.2	C5.3*6.0	Pip die	2.76	1.06	3.16	0.74
2-2	1.5	1.5	(280 ± 30HV10)		2.52	0.98	3.37	0.84
2-3	1.5	2.0			2.57	1.10	3.18	0.92
2-4	1.2	2.0			2.44	1.66	3.06	0.97
2-5	1.8	2.0			2.92	0.98	3.23	0.68
2-6	2.5	2.0			3.45	0.56	3.60	0.38
3-1	1.2	2.0	C5.3*6.0	Flat die	2.68	2.11	2.84	0.93
3-2	1.8	2.0	(280 ± 30HV10)		3.16	1.61	2.94	0.78
3-3	2.5	2.0			3.65	0.74	3.28	0.49

$$\theta_1 = \arccos\left(\frac{l_2}{l_3}\right) \tag{24}$$

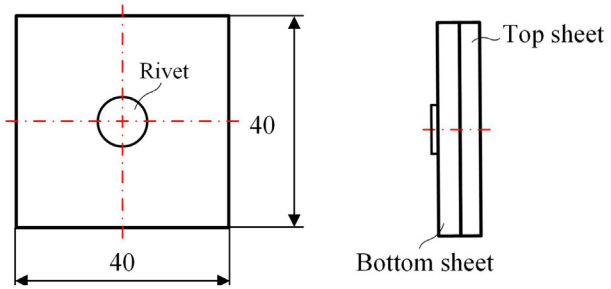

Fig. 31. Specimen size of the SPR joint (in mm).

For the S_1, S_2, R_{in} and I_m, the observation directions (A or B) would not affect the measured values of the R_{in} and I_m but would influence the values of the S_1 and S_2. When observing the joint cross-sectional profile along the direction vertical to the joint central plane (Direction A), the positions of interlock boundaries along the vertical direction would not be affected by the Δh and θ_1. In other word, the measured S_1 and S_2 will be exactly equal to the values on the joint central plane. In contrast, when observing the joint cross-sectional profile along the direction vertical to the cutting plane (Direction B), the positions of interlock boundaries would be affected by the Δh and θ_1. As a result, the measured S_1 and S_2 became slightly larger than the values on the joint central plane. Therefore, it is suggested to measure these four parameters on the joint cross-sectional profile captured along the direction A. Moreover, it is also worth noticing that, compared with the joint profile captured from the direction A, the joint profile captured from the direction B was slightly stretched along the vertical direction, as shown in

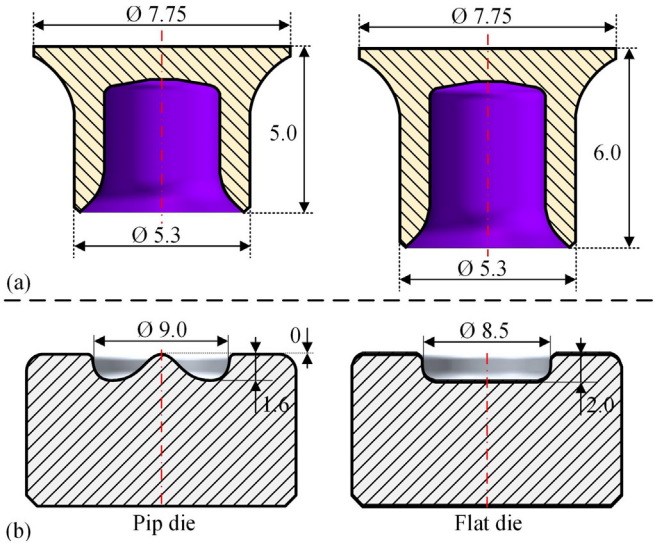

Fig. 32. Dimensions of the (a) semi-tubular rivets and (b) dies (in mm).

Fig. 29(d). This leads to a larger distortion of the captured joint cross-sectional profile, and would affect the quality evaluation of the deformed bottom sheet. Therefore, it is recommended to inspect the joint cross-sectional profile along the direction A and then evaluate the joint quality.

5. Assessment of the proposed estimation and correction methods

Using the proposed approach, the cutting position's influences on the measurement accuracy of interlock in real SPR joints were estimated. The effectiveness of the developed interlock error correction method was also verified.

5.1. Development of graphical user interface (GUI)

For an easier use in practical applications, two graphical user interfaces (GUI) for the interlock error estimation and correction were developed using the App Designer in MATLAB R2018a, as shown in Fig. 30. In the GUI for interlock error correction, the initial interlock errors of the sectioned SPR joint were also calculated. The two GUIs were used in the following sections.

5.2. Experiment design

Ø5.3 mm boron steel rivets (Hardness: 280 ± 30HV10) and aluminium alloy AA5754 sheets were used throughout the experiment. Fifteen SPR joints with different configurations were made as listed in Table 1. The top sheet thickness (T_t), bottom sheet thickness (T_b), rivet length (L_1) and die type varied from joint to joint. Li et al. [26] reported that the rivet to sheet edge distance could affect the joint quality by altering the sheet distortion levels. To avoid this phenomenon, the specimen size used in this study is 40 mm × 40 mm as presented in Fig. 31. Fig. 32 illustrates the dimensions of the rivets and dies used in the experimental SPR tests. The intrinsic variability of the SPR process inevitably brings many variations into the joining process and thus affects the final laboratory test results. To minimise such effects, repeated trials were usually performed when evaluating the SPR joint quality [27]. However, this study focused on the measurement error for the individual joint, and thus only one sample was made for each joint configuration. All the fifteen joints were manufactured using a servo SPR system manufactured by Tucker GmbH, as shown in Fig. 33. This riveting system is displacement controlled rather than pressure controlled, and therefore the rivet head heigh (H_1) was set to 0.0 mm for all the joints. The riveting speed is 300 mm/s, and the clamping force of the blank-holder is approx. 6.0kN.

All the specimens were sectioned using an abrasive-wheel cutting machine. To ensure the cutting plane is as close as possible to the joint centre plane, the specially designed fixtures for the 40 mm × 40 mm specimen were used during the riveting and the cutting processes. Usage of fixtures was also reported during the fabrication and cutting processes of SPR joints in [26]. The cross-sectional profile for each joint was captured using an optical microscope after the surface

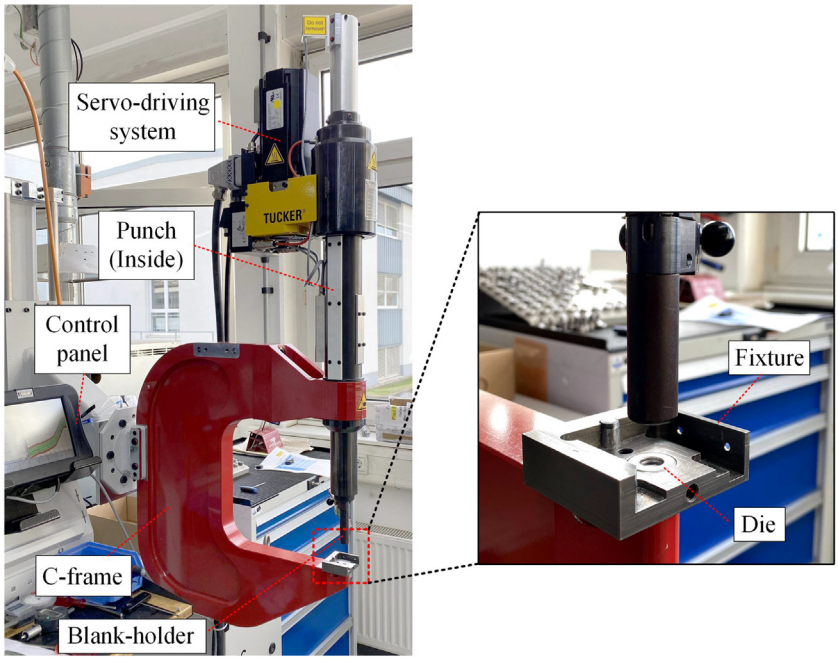

Fig. 33. Structure of the Tucker SPR system.

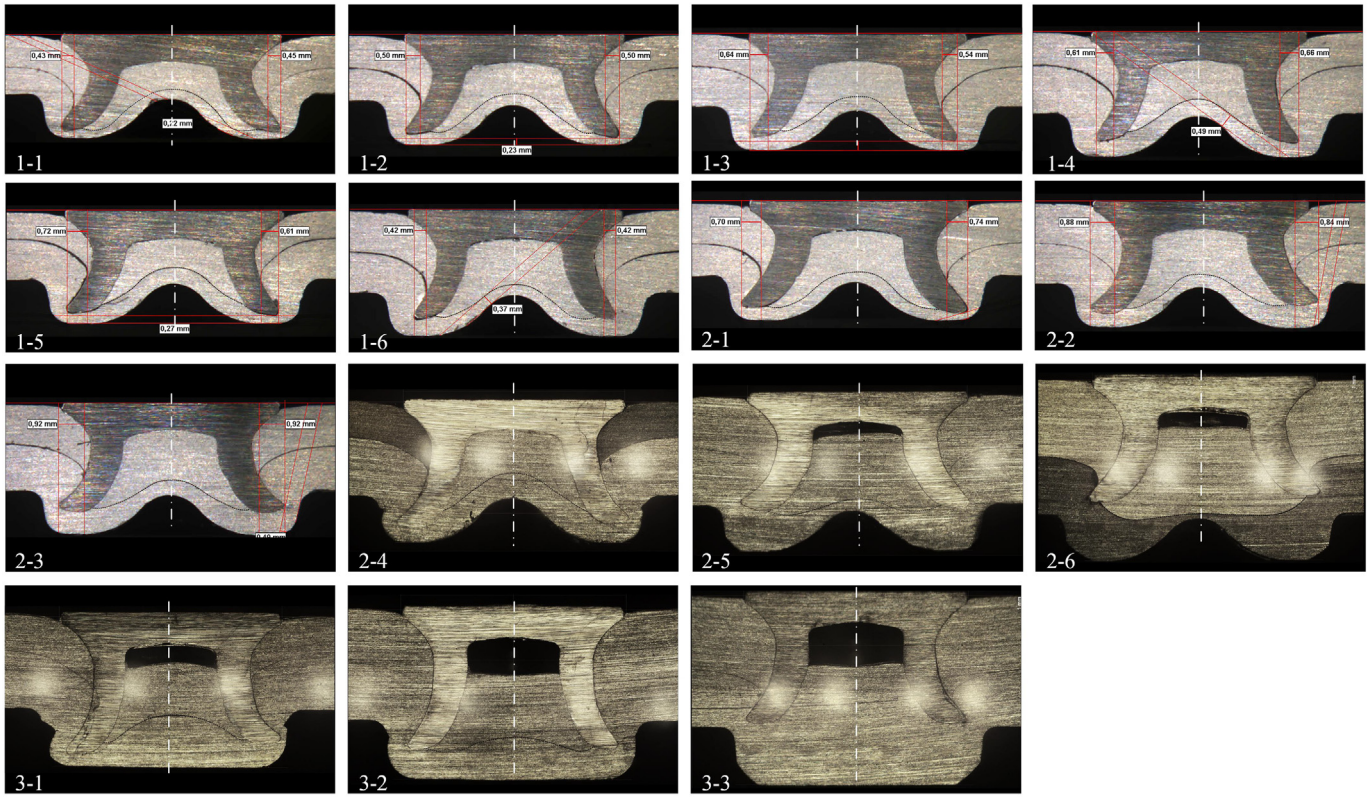

Fig. 34. Joint cross-sectional profiles from experimental SPR tests.

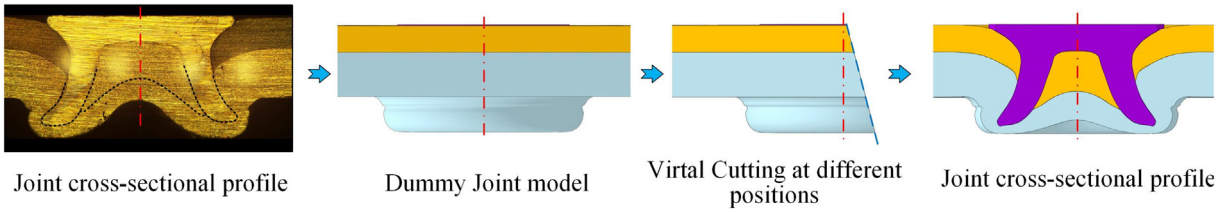

Fig. 35. Procedures to virtually cut the SPR joint at different cutting positions and capture the corresponding cross-sectional profiles.

polishing. The experimentally captured fifteen joint sectional profiles are shown in Fig. 34, and all of them were assumed to be the true joint profiles on the joint central plane. The necessary dimensions, including the S_1, S_2, $R_{\text{in-true}}$ and I_{true}, were measured and recorded in Table 1. Then, the interlock errors for each SPR joint were estimated if these joints were improperly sectioned at different cutting positions.

To verify the performance of the proposed interlock correction method, each SPR joint should be sectioned at different cutting positions. However, because every experimentally fabricated SPR joint is unique, it is very difficult to experimentally cut one SPR joint at different cutting positions (e.g. Ten positions) and observe the cross-sectional profiles. In order to overcome this difficulty, an alternative approach was proposed as shown in Fig. 35. Firstly, a 2D geometry of the experimentally captured joint cross-sectional profile was extracted and used to establish a 3D dummy SPR joint in SolidWorks 2018. Then, this dummy joint was sectioned at different cutting positions, and the corresponding joint cross-sectional profiles were recorded. Finally, the interlock error at each cutting position was accessed and compensated using the proposed error correction method. The developed dummy model may be not exactly the same to the experimentally tested one, while this would not affect the performance assessment of the proposed interlock error correction method. In this study, taking the joint 2–4 as an example, the performance of the proposed interlock correction method was evaluated. The dummy joint 2–4 was sectioned at ten different cutting positions as listed in Table 2 and the necessary data (i.e. S_1, S_2, I_m and R_{in}) was collected from the captured joint cross-sectional profiles. The P0 is the referenced cutting position ($\Delta h = 0$ mm, $\theta_1 =$

Table 2
Ten cutting positions of the dummy joint 2–4.

Position no.	Offset distance Δh (mm)	Rotation angle θ_1 (°)
P0	0.0	0.0
P1	0.5	5.0
P2	0.5	10.0
P3	0.5	15
P4	1.0	5.0
P5	1.0	10
P6	1.0	15
P7	1.5	5.0
P8	1.5	10
P9	1.5	15

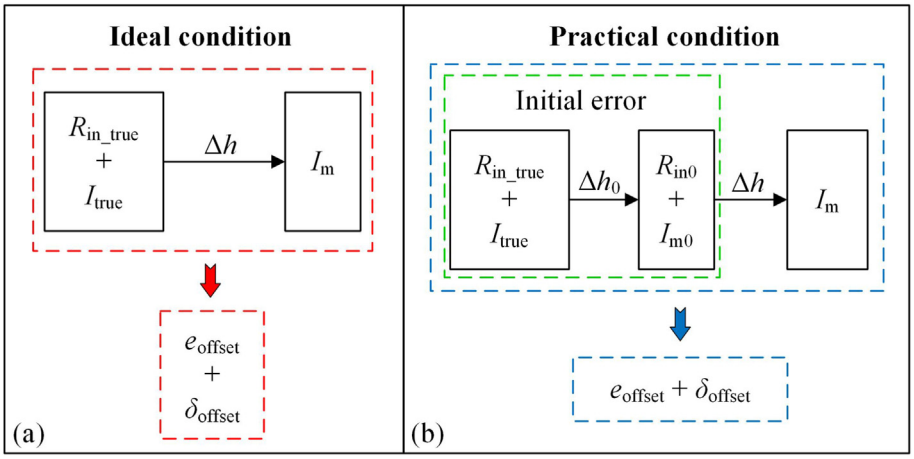

Fig. 36. Estimation of interlock errors caused by the offset distance (Δh) under the (a) ideal condition and (b) practical condition.

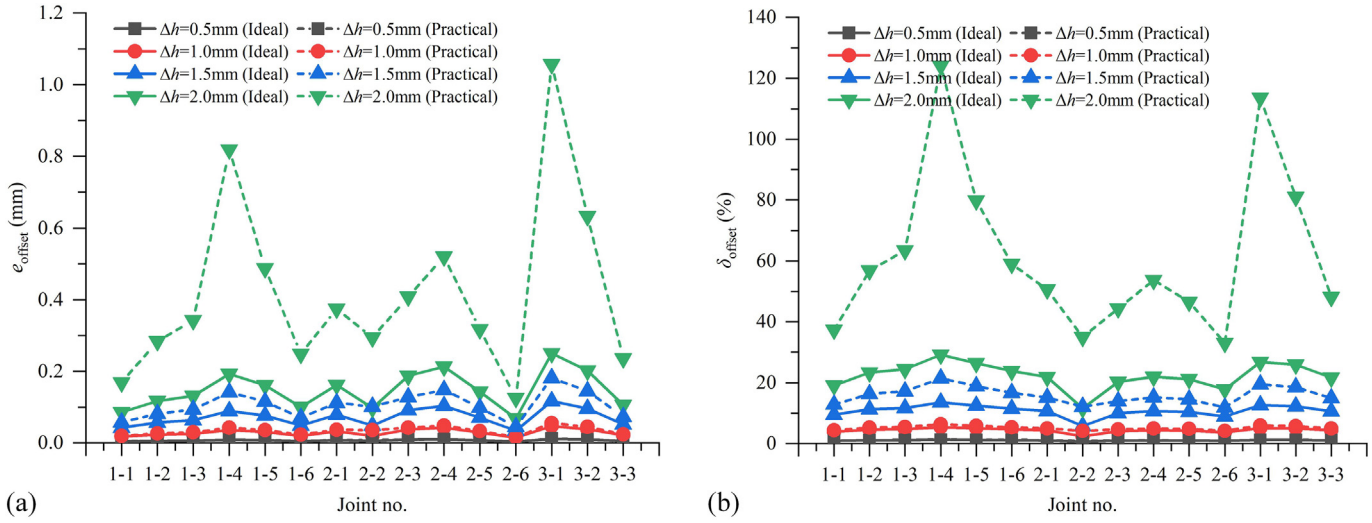

Fig. 37. Estimated (a) Absolute error e_{offset} and (b) Relative error δ_{offset} of the tested SPR joints with different offset distances (Δh).

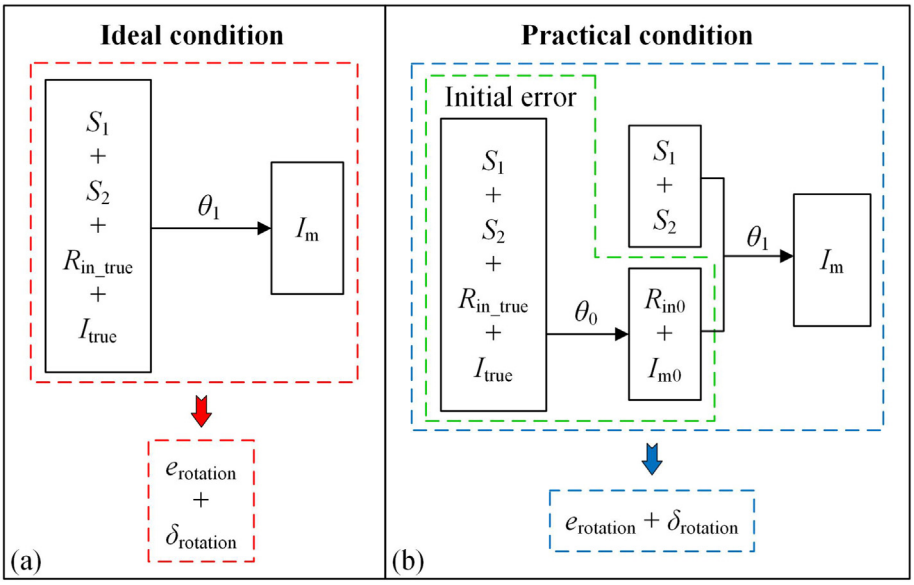

Fig. 38. Estimation of interlock errors caused by the rotation angle (θ_1) under the (a) ideal condition and (b) practical condition.

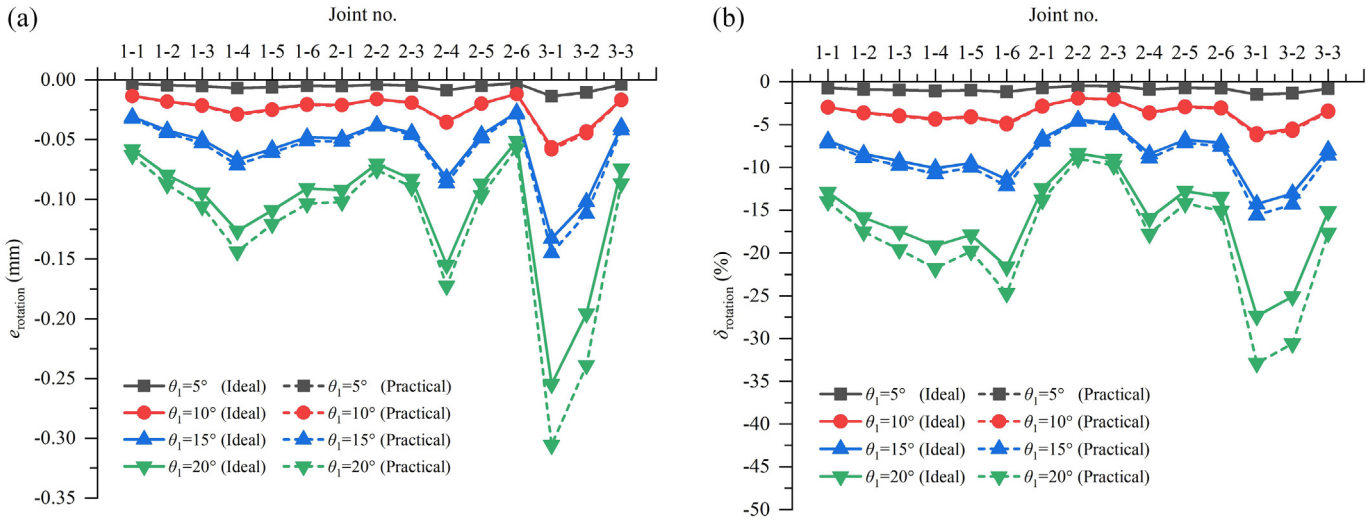

Fig. 39. Estimated (a) Absolute error $e_{rotation}$ and (b) Relative error $\delta_{rotation}$ of the 15 SPR joints with different rotation angles (θ_1).

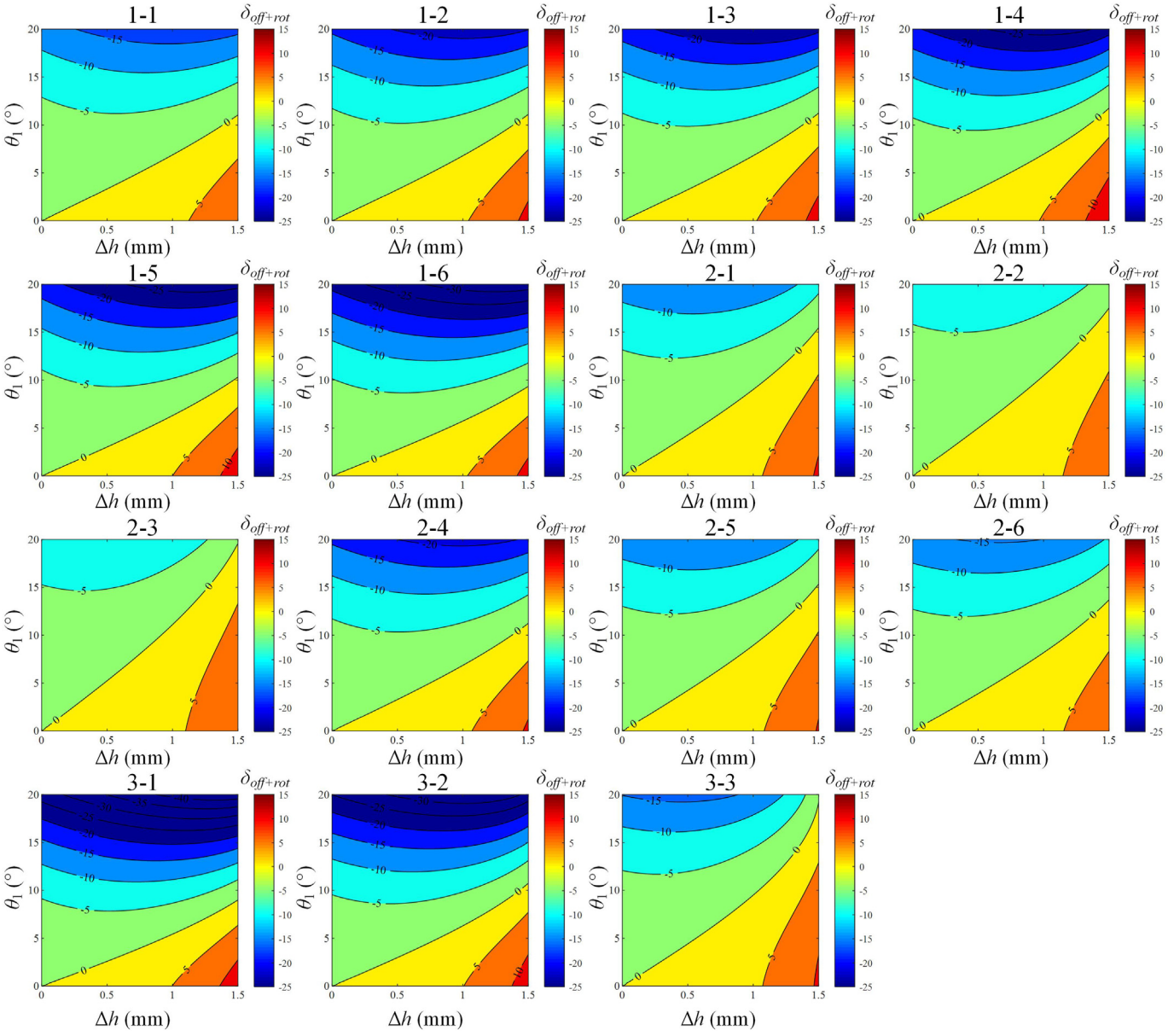

Fig. 40. Relative error ($\delta_{off+rot}$) of interlock in the 15 SPR joints with varying offset distance (Δh) and rotation angle (θ_1).

0). Finally, the measured interlock from the rest nine positions was corrected and compared with the interlock at the position P0.

5.3. Results and discussions

5.3.1. Interlock error with only the offset distance (Δh)

Based on the proposed approach, as shown in Fig. 36(a), the R_{in_true} and I_{true} from the joint central plane should be used to evaluate the influences of the Δh on the measurement errors of the interlock. Under this ideal condition, a Δh was introduced into the $R_{in\text{-}true}$ and I_{true} to calculate the I_m by Eq. (1). Then, the δ_{offset} and e_{offset} were estimated with the I_{true} and the I_m. However, in practice, the R_{in_true} and I_{true} cannot be experimentally measured even with the assistance of specially designed fixtures [25]. To verify the effectiveness of the proposed assessment method under practical conditions, as shown in Fig. 36(b), an initial error was considered by introducing an initial offset distance (Δh_0). The calculated initially measured radius of inner interlock boundary (R_{in0}) and the initially measured interlock (I_{m0}) were regarded as the experimentally measured values. R_{in0} can be obtained by Eq. (25) according to the geometrical relationships shown in Fig. 19. Then, a Δh was introduced into the R_{in0} and I_{m0}, and the corresponding δ_{offset} and e_{offset} were evaluated using the calculated I_{m0} and the I_m.

$$R_{in0} = \sqrt{R_{in-true}^2 - (\Delta h + S_1 \cdot \tan\theta_1)^2} \tag{25}$$

Fig. 37 shows the calculated δ_{offset} and e_{offset} under the ideal condition (Solid lines) and the practical condition (Dash lines) for the 15 SPR joints in Table 1. For simplicity, the Δh_0 and Δh were set to same values in this study. It can be seen that, when the Δh equalled to 0.5 mm and 1.0 mm, the δ_{offset} and e_{offset} under the two conditions were almost the same (Black and red lines). The calculated δ_{offset} and e_{offset} under the practical condition were still very close to that under the ideal condition with the Δh increasing to 1.5 mm (Blue lines). However, when the Δh further increased to 2.0 mm, the δ_{offset} and e_{offset} under the practical condition became much larger than that under the ideal condition (Green lines). Therefore, it is reasonable to believe that the error level of interlock can be estimated directly using the experimentally measured R_{in} and I_m as long as the Δh was smaller than 1.5 mm. The e_{offset} fluctuated around 0.01 mm, 0.025 mm and 0.07 mm for the $\Delta h = 0.5$ mm, 1.0 mm and 1.5 mm respectively. This means the measured interlock was always larger than the true interlock when only with the Δh. The δ_{offset} fluctuated around 1%, 5% and 10% for the $\Delta h = 0.5$ mm, 1.0 mm and 1.5 mm respectively. This indicated that the measured interlock can still maintain a very high accuracy if the Δh was smaller than 1.0 mm.

5.3.2. Interlock error with only the rotation angle (θ_1)

When only with the θ_1, the measurement errors of interlock under the ideal and practical conditions for the 15 SPR joints were also calculated and compared. As shown in Fig. 38(a), under the ideal condition, a θ_1 was introduced to calculate the I_m. Then, the I_{true} and the I_m were used to evaluate the $\delta_{rotation}$ and $e_{rotation}$. While under the practical condition, the R_{in_true} and I_{true} cannot be experimentally measured. As shown in Fig. 38(b), an initial error was considered by introducing an initial rotation angle (θ_0). Then, the calculated R_{in0} and I_{m0} were used to calculate the I_m. Finally, the I_{m0} and the I_m were used to calculate the $\delta_{rotation}$ and $e_{rotation}$ under the practical condition.

Fig. 39 shows the evaluated $\delta_{rotation}$ and $e_{rotation}$ under the ideal condition (Solid lines) and the practical condition (Dash lines) for the 15 SPR joints. For simplicity, the θ_0 and θ_1 were set to the same values in this study. It is obvious that the calculated $\delta_{rotation}$ and $e_{rotation}$ under the two conditions were almost the same when the θ_1 equalled to 5°, 10° and 15° (Black, red and blue lines). While when the θ_1 increased to 20°, the calculated $e_{rotation}$ and $\delta_{rotation}$ under the practical condition were still very close to that under the ideal condition in most SPR joints (Green lines). Therefore, it is reasonable to believe that the error level of interlock can be estimated directly using the experimentally measured R_{in} and I_m as long as the θ_1 was smaller than 15°. The $e_{rotation}$ fluctuated around −0.01 mm, −0.02 mm and − 0.05 mm for $\theta_1 = 5°$, 10° and 15° respectively. The $\delta_{rotation}$ fluctuated around −1%, −4% and − 10% for $\theta_1 = 5°$, 10° and 15° respectively. This suggested that the measured interlock with only the θ_1 was always smaller than the true interlock. Meanwhile, the interlock error could be maintained at a low level if the θ_1 was controlled smaller than 10° in practical applications.

5.3.3. Interlock error with the offset distance (Δh) and rotation angle (θ_1)

When the Δh and θ_1 vary within the ranges of 0.0 mm–1.5 mm and 0°–20°, the contour graphs of the relative error ($\delta_{off+rot}$) of interlock for the 15 tested SPR joints were calculated and recorded in Fig. 40. By

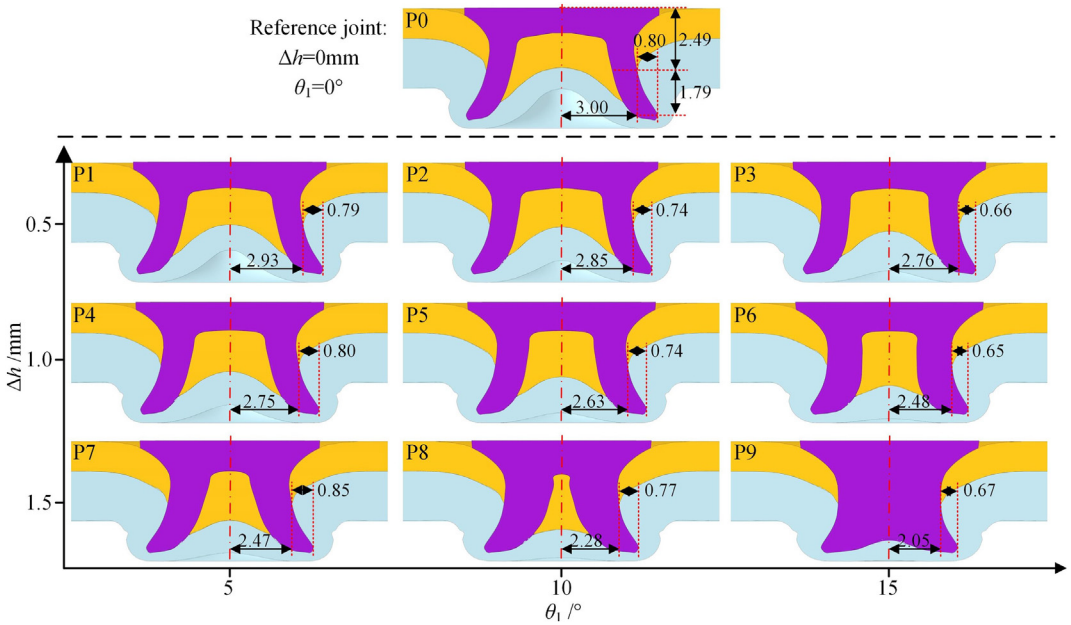

Fig. 41. Cross-sectional profiles of the dummy joint 2–4 at the ten different cutting positions.

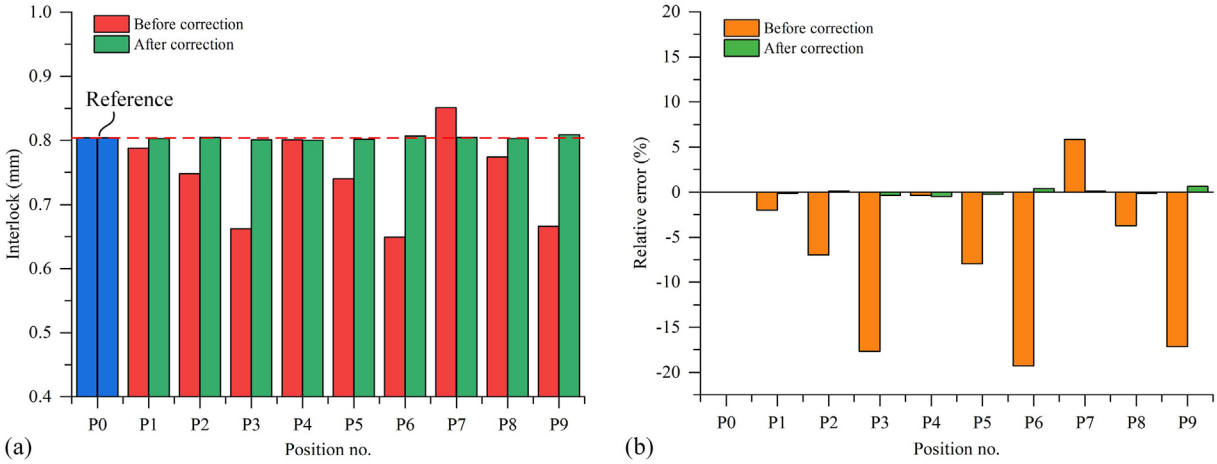

Fig. 42. Comparison of the (a) interlock and (b) relative error at the ten cutting positions of the dummy joint 2–4.

comparing the 15 contour graphs, similar changing patterns of the $\delta_{off+rot}$ were found. The Δh and θ_1 imposed opposite effects on the interlock within the studied ranges. The appearance of θ_1 compensated part of the interlock error caused by the Δh. As a result, the $\delta_{off+rot}$ still maintained at low levels when the effects of the Δh and θ_1 on the interlock were roughly counteracted.

However, in most instances, the influences of the Δh and θ_1 on the interlock were not at the same level. The θ_1 played a leading role on top left portion of the figures and the $\delta_{off+rot}$ always had a negative value. Gradient densities of this region in the 15 contour figures were slightly different: SPR joints with the interlock formation position far away from the rivet head (i.e. large S_1 and S_2) but close to the joint axis (i.e. small $R_{\text{in\_true}}$) were more sensitive to the θ_1 and had a higher gradient density. In contrast, the Δh showed a dominant influence on the bottom right portion of these figures and the $\delta_{off+rot}$ always had a positive value. The gradient densities of this region were almost the same in all the 15 joints. This is because the impacts of Δh on the interlock is only influenced by the $R_{\text{in\_true}}$ and I_{true}. The $R_{\text{in\_true}}$ and I_{true} in the 15 joints changed within relatively small ranges as listed in Table 1, and therefore resulted in similar gradient densities of $\delta_{off+rot}$. It was also found that the accuracy of interlock was just slightly affected by the improper cutting position ($\delta_{off+rot} \approx -5\%$–$5\%$.) if the Δh and θ_1 could be controlled smaller than 1.0 mm and 10° respectively. Although a positive θ_1 could compensate the interlock error caused by the Δh, it would lead to more missing data of the bottom sheet profile and further worsen the measurement accuracy of the remaining bottom sheet thickness.

5.3.4. Correction of interlock error

Fig. 41 shows the captured cross-sectional profiles of the dummy joint 2–4 at the ten different cutting positions in Table 2. When the Δh was greater than 1.0 mm or the θ_1 was larger than 10°, it can be seen that the joint cross-sectional profiles (i.e. P3, P6–P9) already became very different from the referenced one (i.e. P0). Fig. 42(a) compares the measured interlock values before and after correction. Before correction, the absolute error of the interlock was very obvious in P1–P9, and even reached to around −0.15 mm at the positions P3, P6 and P9. In contrast, after correction using the proposed interlock error correction approach, the absolute error of interlock was effectively reduced to a very small value (Less than 0.03 mm). The interlock at all of the nine positions became almost the same to the referenced P0. It can be seen from Fig. 42(b) that the relative error of interlock reduced to approx. 1%–3% at all of the nine improper cutting positions. The correction results indicated that no matter how large the interlock error induced by the improper cutting position is, the proposed correction method could always effectively compensate it to a very low level. Therefore, the developed interlock error correction method was proved effective and would be very helpful when the SPR joints were not properly sectioned in practical applications, such as SPR joints with irregular shapes extracted from the car BIW structures.

6. Conclusions

In this paper, the influences of the improper joint cutting positions on the SPR joint quality indicators were investigated and discussed. Error evaluation and correction methods for the joint interlock were proposed to minimise the impact of the improper cutting position on its measurement accuracy. Two graphical user interfaces (GUI) were also developed to simplify practical applications. The main conclusions are drawn below:

(1) The offset distance (Δh) and rotation angle (θ_1) between the cutting plane and the joint central plane could significantly influence the measurement accuracy of the interlock and the remaining bottom sheet thickness, but no impact on the measured rivet head height (H_1).

(2) The Δh and θ_1 imposed opposite influences on the interlock: the measured interlock (I_{m}) was always larger than the true interlock (I_{true}) with only the existence of Δh, while the I_{m} was always smaller than the I_{true} with only the existence of θ_1. The interlock error induced by the improper cutting position could still be very small when the effects of the Δh and θ_1 on the interlock were roughly counteracted.

(3) Under the studied joint configurations, the relative error of the interlock could be controlled to approx. -5%–5% if the Δh and θ_1 were smaller than 1.0 mm and 10°. The proposed interlock error correction method showed a very good performance, and effectively reduced the relative error of interlock to around 1%–3%.

(4) The Δh and θ_1 could lead to missing data of the remaining bottom sheet thickness around the joint central area. Only part of the bottom sheet profile can be projected from the joint central plane to the cutting plane. The amount of missing data increased rapidly with the increment of the Δh and θ_1. Distortion occurred on the measured bottom sheet profile during the projection process, and resulted in a higher measurement error of the remaining bottom sheet thickness in the region close to the joint axis than in the region close to the rivet tip. It is difficult to quantitatively evaluate and correct the measurement error of the remaining bottom sheet thickness caused by the improper cutting position.

(5) The developed graphical user interface (GUI) facilitates the measurement error evaluation and correction of the interlock in practical applications.

CRediT authorship contribution statement

Yunpeng Liu: Methodology, Writing-original draft, Writing-review & editing, Investigation. **Li Han:** Supervision, Writing-review & editing. **Huan Zhao:** Methodology, Writing-review & editing, Investigation. **Xianping Liu:** Supervision, Project administration, Funding acquisition.

Data availability statement

The raw/processed data required to reproduce these findings cannot be shared at this time as the data also forms part of an ongoing study.

Declaration of Competing Interest

The authors declare that they have no known competing financial interests or personal relationships that could have appeared to influence the work reported in this paper.

Acknowledgements

This research is sponsored by Jaguar Land Rover. The authors would like to thank Dr. Matthias Wissling, Paul Bartig and their team members from Tucker GmbH for their supports during the laboratory tests.

References

[1] H. Jiang, S. Gao, G. Li, J. Cui, Structural design of half hollow rivet for electromagnetic self-piercing riveting process of dissimilar materials, Mater. Des. 183 (2019) 108141, https://doi.org/10.1016/j.matdes.2019.108141.
[2] X. He, L. Zhao, C. Deng, B. Xing, F. Gu, A. Ball, Self-piercing riveting of similar and dissimilar metal sheets of aluminum alloy and copper alloy, Mater. Des. 65 (2015) 923–933, https://doi.org/10.1016/J.MATDES.2014.10.002.
[3] Y. Abe, T. Kato, K. Mori, Self-pierce riveting of three high strength steel and aluminium alloy sheets, Int. J. Mater. Form. 1 (2008) 1271–1274, https://doi.org/10.1007/s12289-008-0134-9.
[4] R. Haque, J.H. Beynon, Y. Durandet, Characterisation of force-displacement curve in self-pierce riveting, Sci. Technol. Weld. Join. 2012 (1718) https://doi.org/10.1179/1362171812Y.0000000036.
[5] Y. Liu, H. Li, H. Zhao, X. Liu, Effects of the die parameters on the self-piercing riveting process, Int. J. Adv. Manuf. Technol. 105 (2019) 3353–3368, https://doi.org/10.1007/s00170-019-04567-4.
[6] L. Fratini, V.F. Ruisi, Self-piercing riveting for aluminium alloys-composites hybrid joints, Int. J. Adv. Manuf. Technol. 43 (2009) 61–66, https://doi.org/10.1007/s00170-008-1690-3.
[7] Y. Abe, T. Kato, K. Mori, Self-piercing riveting of high tensile strength steel and aluminium alloy sheets using conventional rivet and die, J. Mater. Process. Technol. 209 (2009) 3914–3922, https://doi.org/10.1016/j.jmatprotec.2008.09.007.
[8] Y. Ma, M. Lou, Y. Li, Z. Lin, Effect of rivet and die on self-piercing rivetability of AA6061-T6 and mild steel CR4 of different gauges, J. Mater. Process. Technol. 251 (2018) 282–294, https://doi.org/10.1016/J.JMATPROTEC.2017.08.020.
[9] D.H. Kam, T.E. Jeong, M.G. Kim, J. Shin, Self-piercing riveted joint of vibration-damping steel and aluminum alloy, Appl. Sci. 9 (2019) https://doi.org/10.3390/app9214575.
[10] N.-H. Hoang, R. Porcaro, M. Langseth, A.-G. Hanssen, Self-piercing riveting connections using aluminium rivets, Int. J. Solids Struct. 47 (2010) 427–439, https://doi.org/10.1016/J.IJSOLSTR.2009.10.009.
[11] S.N. Van Hall, K.O. Findley, A.K. Freis, Improved self-pierce rivet performance through intentional decarburization, J. Mater. Process. Technol. 251 (2018) 350–359, https://doi.org/10.1016/J.JMATPROTEC.2017.08.018.
[12] D.Z. Li, L. Han, M. Shergold, M. Thornton, G. Williams, Influence of rivet tip geometry on the joint quality and mechanical strengths of self-piercing riveted aluminium joints, Mater. Sci. Forum 765 (2013) 746–750, https://doi.org/10.4028/www.scientific.net/MSF.765.746.
[13] J.H. Deng, F. Lyu, R.M. Chen, Z.S. Fan, Influence of die geometry on self-piercing riveting of aluminum alloy AA6061-T6 to mild steel SPFC340 sheets, Adv. Manuf. 7 (2019) https://doi.org/10.1007/s40436-019-00250-9.
[14] C.G. Pickin, K. Young, I. Tuersley, Joining of lightweight sandwich sheets to aluminium using self-pierce riveting, Mater. Des. 28 (2007) 2361–2365, https://doi.org/10.1016/j.matdes.2006.08.003.
[15] J. Liang, H. Jiang, J. Zhang, X. Wu, X. Zhang, G. Li, J. Cui, Investigations on mechanical properties and microtopography of electromagnetic self-piercing riveted joints with carbon fiber reinforced plastics/aluminum alloy 5052, Arch. Civ. Mech. Eng. 19 (2019) 240–250, https://doi.org/10.1016/J.ACME.2018.11.001.
[16] D. Li, Influence of local surface texture by tool impression on the self-piercing riveting process and the static lap shear strength, J. Manuf. Process. 29 (2017) 298–309, https://doi.org/10.1016/j.jmapro.2017.08.003.
[17] M.A. Karim, T.E. Jeong, W. Noh, K.Y. Park, D.H. Kam, C. Kim, D.G. Nam, H. Jung, Y. Do Park, Joint quality of self-piercing riveting (SPR) and mechanical behavior under the frictional effect of various rivet coatings, J. Manuf. Process. 58 (2020) 466–477, https://doi.org/10.1016/j.jmapro.2020.08.038.
[18] D. Li, A. Chrysanthou, I. Patel, G. Williams, Self-piercing riveting-a review, Int. J. Adv. Manuf. Technol. 92 (2017) 1777–1824, https://doi.org/10.1007/s00170-017-0156-x.
[19] R. Haque, Quality of self-piercing riveting (SPR) joints from cross-sectional perspective: a review, Arch. Civ. Mech. Eng. 18 (2018) 83–93, https://doi.org/10.1016/j.acme.2017.06.003.
[20] L. Han, M. Thornton, D. Li, M. Shergold, Effect of setting velocity on self-piercing riveting process and joint behaviour for automotive applications, SAE Tech. Pap. (2010) https://doi.org/10.4271/2010-01-0966.
[21] X. Zhang, X. He, B. Xing, W. Wei, J. Lu, Quasi-static and fatigue characteristics of self-piercing riveted joints in dissimilar aluminium-lithium alloy and titanium sheets, J. Mater. Res. Technol. (2020) https://doi.org/10.1016/j.jmrt.2020.03.095.
[22] L. Huang, J.F.C. Moraes, D.G. Sediako, J.B. Jordon, H. Guo, X. Su, Finite-element and residual stress analysis of self-pierce riveting in dissimilar metal sheets, J. Manuf. Sci. Eng. 139 (2016), 021007, https://doi.org/10.1115/1.4034437.
[23] F. Hirsch, S. Müller, M. Machens, R. Staschko, N. Fuchs, M. Kästner, Simulation of self-piercing rivetting processes in fibre reinforced polymers: material modelling and parameter identification, J. Mater. Process. Technol. 241 (2017) 164–177, https://doi.org/10.1016/j.jmatprotec.2016.10.010.
[24] A. Rusia, S. Weihe, Development of an end-to-end simulation process chain for prediction of self-piercing riveting joint geometry and strength, J. Manuf. Process. 57 (2020) 519–532, https://doi.org/10.1016/j.jmapro.2020.07.004.
[25] T. Gerstmann, B. Awiszus, Hybrid joining: numerical process development of flat-clinch-bonding, J. Mater. Process. Technol. 277 (2020) 116421, https://doi.org/10.1016/j.jmatprotec.2019.116421.
[26] D. Li, L. Han, M. Thornton, M. Shergold, Influence of edge distance on quality and static behaviour of self-piercing riveted aluminium joints, Mater. Des. 34 (2012) 22–31, https://doi.org/10.1016/j.matdes.2011.07.046.
[27] H. Zhao, L. Han, Y. Liu, X. Liu, Modelling and interaction analysis of the self-pierce riveting process using regression analysis and FEA, Int. J. Adv. Manuf. Technol. (2021) 1–18, https://doi.org/10.1007/s00170-020-06519-9.